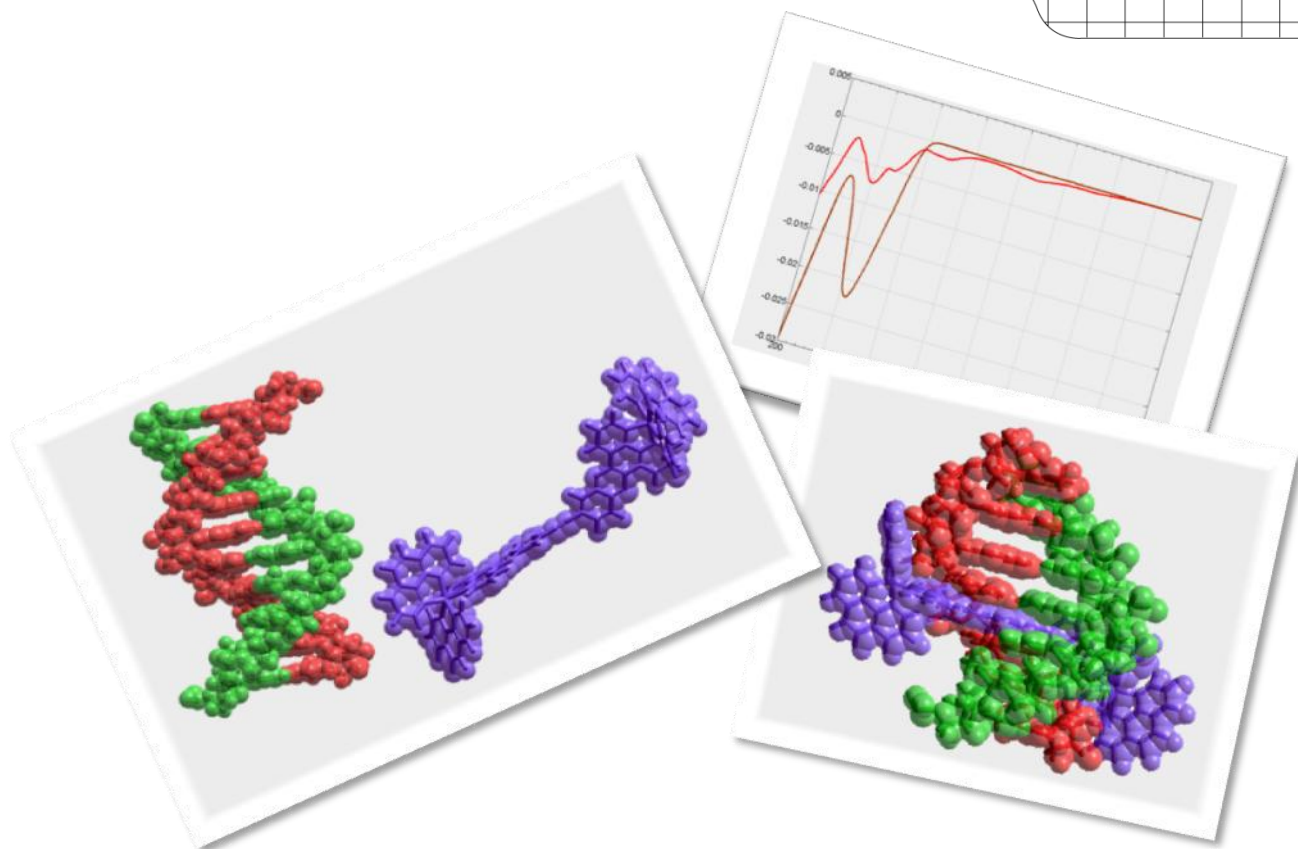


# CHALMERS



## **Biophysical investigation of the DNA interaction of a new binuclear ruthenium complex**

**Master of Science Thesis**

**Yubo Wang**

Department of Chemical and Biological Engineering  
*Division of Chemistry and Biochemistry, Physical Chemistry*  
CHALMERS UNIVERSITY OF TECHNOLOGY  
Göteborg, Sweden, 2010



THESIS FOR THE DEGREE OF MASTER OF SCIENCE

Biophysical investigation of the DNA interaction  
of a new binuclear ruthenium complex

Yubo Wang



**CHALMERS**

Department of Chemical and Biological Engineering

CHALMERS UNIVERSITY OF TECHNOLOGY

Göteborg, Sweden 2010

# Biophysical investigation of the DNA interaction of a new binuclear ruthenium complex

©Yubo Wang, 2010

Department of Chemical and Biological Engineering

Chalmers University of Technology

SE-412 96 Göteborg

Sweden

Tel. +46 (0) 31 772 10 00

Cover pictures: left: three dimensional model of B-DNA and Complex PA; right bottom: three dimensional model of the threading intercalation of D-DNA and Complex PA; right top: the LD spectra of *calf thymus* DNA and Complex  $\Delta,\Delta$ -PA bind to *calf thymus* DNA

Department of Chemical and Biological Engineering

Göteborg, Sweden 2010

# Biophysical investigation of the DNA interaction of a new binuclear ruthenium complex

Yubo Wang

Department of Chemical and Biological Engineering

Chalmers University of Technology

## Abstract

50 years since the structure of DNA was proposed, DNA-interactive agents are still an intense field of study. Transition metal complexes possess many features that make them interesting as DNA-interactive compounds, and many have been studied as cytotoxic agents and anticancer drugs. Ruthenium (II) chiral tris-chelate complexes with different DNA affinitive ligands have been studied for more than 20 years, recently, binuclear ruthenium complexes, in particular, increasingly become a major focus due to their sequence selective binding mode of threading intercalation. In this thesis, the DNA binding properties of a new binuclear ruthenium complex  $[\mu\text{-(bidppz acetylene)(phen)}_4\text{Ru}_2]^{4+}$  (PA) with an elongated bridge group compared with the parent binuclear ruthenium complex  $[\mu\text{-(bidppz)(phen)}_4\text{Ru}_2]^{4+}$  (P) has been studied. The binding mode and the kinetic selectivity were investigated.

The binding modes of the two enantiomers of PA show huge differences. For  $\Delta,\Delta$ -PA, threading intercalation is seems to be the main binding mode, but for  $\Lambda,\Lambda$ -PA, the experiment reveals no threading intercalation with DNA. The threading kinetics of  $\Delta,\Delta$ -PA is less affected by temperature compared with  $\Delta,\Delta$ -P, and the rate of threading intercalation into ct-DNA is faster than for P. Also, the unthreading kinetics is slower for  $\Delta,\Delta$ -PA than for P making  $\Delta,\Delta$ -PA a stronger threading intercalator than P. On the other hand, the results for poly(dAdT)<sub>2</sub> indicate that  $\Delta,\Delta$ -PA will have a lower sequence selectivity compared to the parent  $\Delta,\Delta$ -P. The finding that by altering the bridge group of binuclear ruthenium complexes, the enantiomer selectivity will vary, will be an interesting point for future study.

Key words: DNA, ruthenium complex, intercalation, kinetics, sequence selectivity, spectroscopy, absorption, fluorescence, linear dichroism, circular dichroism

## Abbreviations List

CD	Circular Dichroism
ct-DNA	<i>Calf thymus</i> DNA
DD	$\Delta, \Delta$ (only showed in Figures)
DNA	Deoxyribonucleic acid
Dppz	Dipyrido[3,2-a:2',3'-c]phenazine
KACK	Dimethylarsinic acid
LD	Linear Dichroism
LDr	Reduced LD
LL	$\Lambda, \Lambda$ (only showed in Figures)
MLCT	Metal-to-Ligand Charge Transfer
mRNA	Messenger Ribonucleic Acid
NaCl	Sodium Chloride
P	$[\mu\text{-(bidppz)(phen)}_4\text{Ru}_2]^{4+}$
PA	$[\mu\text{-(bidppz acetylene)(phen)}_4\text{Ru}_2]^{4+}$
Phen	1,10-N,N-Phenanthroline
RNA	Ribonucleic Acid
SDS	Sodium dodecyl sulphate

## Content

Content.....	i
1. Introduction.....	1
2. Theory.....	3
2.1 Nucleic acid.....	3
2.1.1 DNA Structure.....	4
2.1.2 AT-Rich DNA.....	5
2.1.3 DNA-Ligand Interactions.....	5
2.2 Ruthenium Complexes.....	7
2.4 Spectroscopy.....	9
2.4.1 Absorption and Fluorescence.....	10
2.4.2 Time-Domain Lifetime Measurement.....	11
2.5 Polarized Spectroscopy.....	13
2.5.1 Linear Dichroism.....	13
2.5.2 Circular Dichroism.....	15
2.6 Kinetics of Chemical Reactions.....	15
3. Material and Methods.....	19
3.1 Sample preparation.....	19
3.1.1 Buffer.....	19
3.1.2 Ruthenium complexes.....	19
3.1.3 DNA.....	19
3.1.4 Mixing.....	19
3.2 Absorption.....	20
3.3 Linear Dichroism.....	20
3.4 Fluorescence.....	20
3.5 Fluorescence Lifetime Measurement.....	20
3.6 Analysis of Kinetics Data and Decay Time.....	21
4. Results and Discussions.....	23

4.1 Experiment Conditions.....	23
4.2 Absorption.....	23
4.3 Circular Dichroism.....	24
4.4 Linear Dichroism.....	25
4.5 Reduced Linear Dichroism.....	27
4.6 Fluorescence.....	28
4.7 Fluorescence Lifetime Measurement .....	28
4.8 Binding Mode Summary .....	29
4.9 Association Kinetic .....	29
4.10 Dissociation Kinetics.....	33
5. Conclusion .....	37
5.1 Binding Mode.....	37
5.2 Kinetics.....	37
6. Acknowledgement .....	39
7. References.....	41
Appendix I .....	45
Appendix II.....	49

## 1. Introduction

Despite the amazing variety of living organisms on Earth, they are all, from tiny bacteria ( $\mu\text{m}$ ) to large plants and animals, built based on the same small unit, the cell. The genetic mystery, with the conservational features and evolutionary mutations of each generation, has obsessed human for thousands of years. Not until nucleic acids was firmly established as the main genetic material in living cells in 1952[1], the enigma of heredity was disclosed. Deoxyribonucleic acid, DNA, is the carrier of the genetic information and plays an important role in all living organisms. One year later in 1953, the DNA double helix structure was demonstrated by James D. Watson and Francis H. C. Crick [2]. These breakthroughs symbolized a significant milestone of human scientific development during the 20th century.

The genetic information is encoded in the DNA double helix which serves as the template for protein synthesis by transcription of DNA into messenger ribonucleic acid (mRNA). Subsequently, mRNA is, in the ribosome, [3-4] translated into the amino acids sequences, which after folding into the correct 3-dimensional structure becomes a functional protein expressing the biological features. The sequences of the 46 chromosomes in human being have been surveyed via an international collaboration, the Human Genome Project, and were published in *Nature* [5] and *Science* [6] in 2001.

Since DNA functions as a “terminal controller” of the human life, theoretically, every disease and disorder of the body should match to an error in the corresponding DNA code region. Nowadays, proteins are still a popular target for disease therapy, but the activities of proteins can also be altered by DNA- targeting drugs at the transcription level[7]. DNA-targeted therapeutic regulation is a strategy of curing genetic diseases, such as cancer [8-11]. Small molecules that bind to DNA play an important role to control the protein expression and cell cycles with the purpose to inhibit uncontrolled cell proliferation and other genetic diseases. In order to be able to cure genetic diseases without threatening normal cells the most challenging task is to design a specific DNA-targeted molecule which could bind to specific DNA sequences. Particularly, the chemical and physical properties are two of the most important factors to select small molecules as DNA-binding drugs. Distinguishing between the normal and cancerous cells is also a crucial point because the normal and cancerous cells are remarkably similar, and most anticancer drugs manifest adverse side effects[9]. Recently, transition metal complexes have been reported to act as highly efficient anticancer drugs which have special selectivity for cancerous cells as the target [10-11].

In the total different mode of action, threading intercalating binuclear ruthenium complexes, which are substitution inert, have been found to selectively intercalate into AT-rich DNA.

In this thesis, two different enantiomers of a new binuclear ruthenium complex, with elongated bridge ligand length, were used to investigate the impact of kinetic selectivity towards calf thymus DNA and poly (dAdT)<sub>2</sub> - DNA, respectively. Temperature, a key point also obviously affects the kinetics of a reaction, was investigated during the thesis.

## 2. Theory

The structure and function of DNA and ruthenium complexes are fundamental in this thesis. In this section, the basic theories of DNA and ruthenium complexes are briefly presented as well as the theory of the methods used in this thesis.

### 2.1 Nucleic acid

Nucleic acid is the generic name for a family of biopolymers, which are biological macromolecules, composed of chains of monomeric nucleotides. Each nucleotide consists of three components: a nitrogenous heterocyclic base, which is either a purine or a pyrimidine, a pentose sugar, and a phosphate group (Fig 2.1a, left). The backbones of the poly nucleotide chains are made of alternating sugars and phosphate groups joined by ester bonds (Fig 2.1a, right). There are two types of nucleic acids that differ in the structure of the sugar in their nucleotides; RNA contains ribose while DNA contains 2-deoxyribose. Also, the nitrogenous base composition found in the two nucleic acid types are somewhat different: adenine (A), cytosine (C) and guanine (G) are found in both RNA and DNA, while thymine (T) only occurs in DNA and uracil (U) only occurs in RNA (Fig 2.1 b).[12]

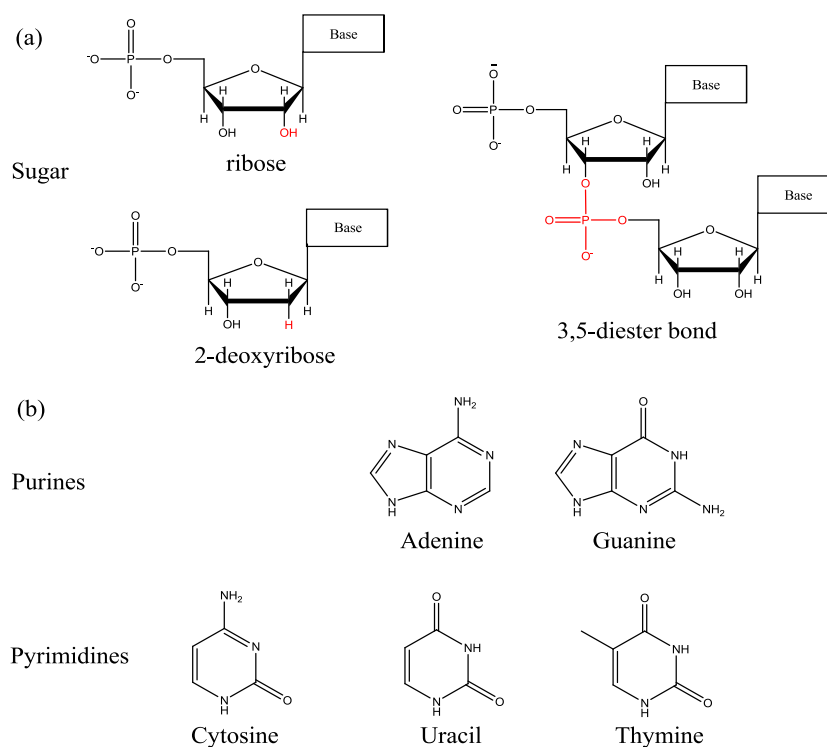


Figure 2.1 (a) the structure of ribose and 2-deoxyribose which are present in RNA and DNA separately; (b) the bases adenine (A), guanine (G), cytosine(C), uracil (U) and thymine (T)

### 2.1.1 DNA Structure

Hydrogen bonding and hydrophobic effects are the dominating forces to connect the two single strands to a double stranded DNA helix, in which A pairs with T by two hydrogen bonds and G binds to C by three hydrogen bonds (Fig 2.2). A-form, B-form and Z-form DNA are attributed to the different geometries of the DNA double helix (Fig 2.3). The DNA helix is unsymmetric, having a broad major groove and narrower minor groove. The phosphate groups carry one negative charge each, making DNA a polyanion at physiological pH. B-form DNA is the most common configuration for natural DNA.

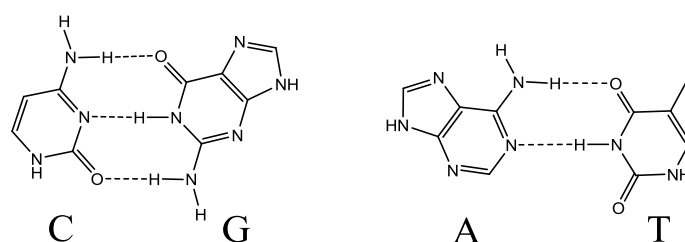


Fig 2.2 DNA base pairing

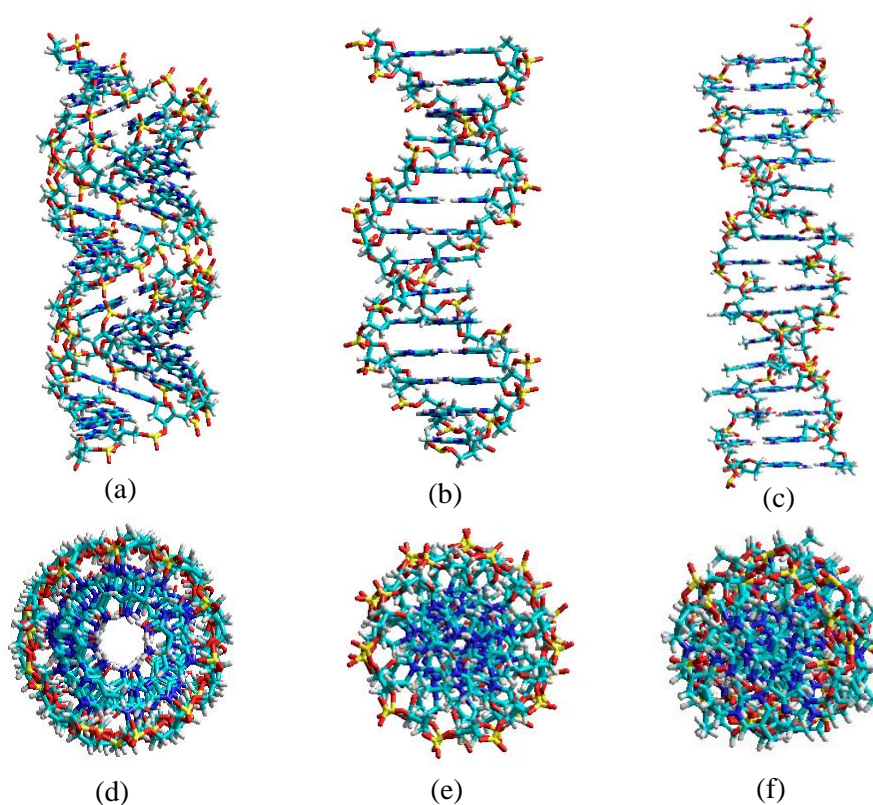


Fig 2.3 side-view and top-view of double-helix structure of 3 forms DNA: (a) A-DNA (b) B-DNA (c) Z-DNA (d) A-DNA (e) B-DNA (f) Z-DNA

(Models are built with HyperChem software)

### 2.1.2 AT-Rich DNA

AT-rich DNA segments, which frame specific gene domains, were discovered more than 20 years ago [13-15]. AT-rich DNA is considered to be of special interest as a target for drugs since it frequently is found at functionally important locations, such as promoter regions and origins of replication[16]. Also, AT-rich DNA is found in human pathogens such as the malaria parasite, including the most lethal *Plasmodium falciparum*, which is becoming increasingly resistant to existing antimalarial drugs. One remarkable opportunity to selectively target *P. falciparum* stems from the unique AT-richness of its genome (80% A/T, relative to 60% in human DNA) [17]. In consequence, studies of the interactions between small DNA-binding molecules and AT-rich DNA are of great significance for DNA-targeting drug research.

### 2.1.3 DNA-Ligand Interactions

Except of the effective cytotoxic agents, someone doubt that the value of developing new DNA targeting agents because of the lack of tumor cell recognition by the DNA-interactive agents [18]. However, the clinical importance of DNA-interactive agents can hardly be overstated as many anticancer regimens include a drug which can bind or modify the DNA molecules. Consequently, studies of DNA-ligand interaction are useful biochemical tools for visualization of DNA both *in vitro* and inside the cell[19]. The non-covalent interaction mode of small molecules with DNA can be classified into three categories: electrostatic interaction, intercalation and groove binding (Fig 2.4).

Due to the configuration of the DNA double helix, the negatively charged phosphate groups which are found in the periphery will attract positively charged groups by coulombic force, so called electrostatic interactions.

In chemistry, intercalation refers to a molecule being inserted between two other molecules or groups, a process that is reversible. There are many molecules that bind between DNA base pairs by intercalation, which result in the length increase and twist decrease of the DNA helix [20]. Usually, intercalators are multi-ring, aromatic or planar structures (Fig 2.5). DNA intercalators are widely used in antitumor, antineoplastic, antimalarial, antibiotic and antifungal agents, however, that does not mean that all intercalators have genotoxicity (defined by the ability to alter the genetic material in cells as a means of inducing a toxic effect) [19, 20].

Groove binding does not, like intercalation, change the configuration of the DNA molecule. Groove binding is more like a standard lock-and-key model, where a bio-macromolecule and a ligand match each other. Common groove binders are usually

crescent-shaped molecules that usually most often prefer to bind the minor groove of DNA (Fig 2.5)[21]. As well as intercalators, groove binders can be used for clinical treatment of cancer and bacterial infections [22]. For instance, the anticancer drug mitomycin is an atypical groove binder and anthracyclines, a class of clinically important compounds with antineoplastic and antibacterial properties, take advantage of both modes of binding as they possess an intercalative unit as well as a groove-binding side chain[23].

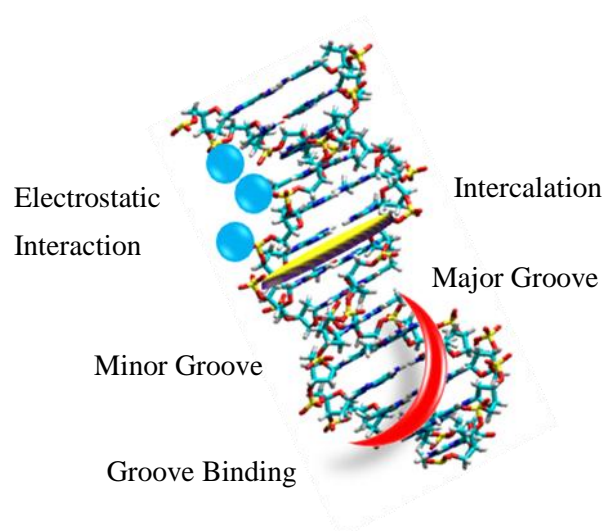
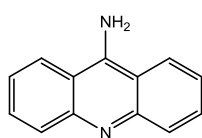
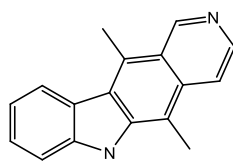


Fig 2.4 Three binding mode

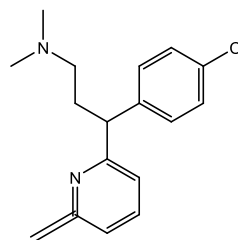
#### Intercalators



9-Aminoacridine

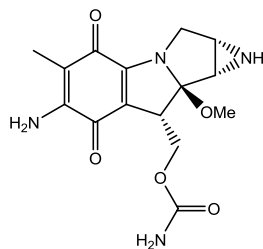


Ellipticine

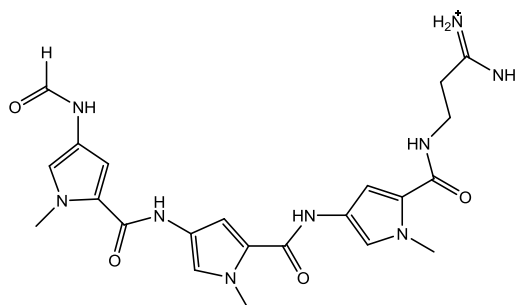


Cholropheniramine

#### Groove Binders



Mitomycin



Distamycin

Fig 2.5 Left: Schematic picture of possibilities of interaction between small molecules and DNA; Right: Structures of intercalators and groove binders

## 2.2 Ruthenium Complexes

Transition metal complexes with ruthenium as central atom and their interactions with DNA are investigated in this project. Prior to this project, extensive research has been done on the interaction between DNA and chiral tris-chelate complexes of transition metals complex [24-26]. Due to the strong binding and serviceable photophysical properties of ruthenium complexes, they are often used as DNA dyes [27-29]. Ruthenium is a transition metal and situated below iron atom in the periodic table, and the divalent Ru(II) ions can perform very stable complexes with bidentate nitrogen ligands such as 1,10-N,N-phenanthroline (phen) and dipyrido[3,2-a:2',3'-c]phenazine (dppz). (Fig 2.6)

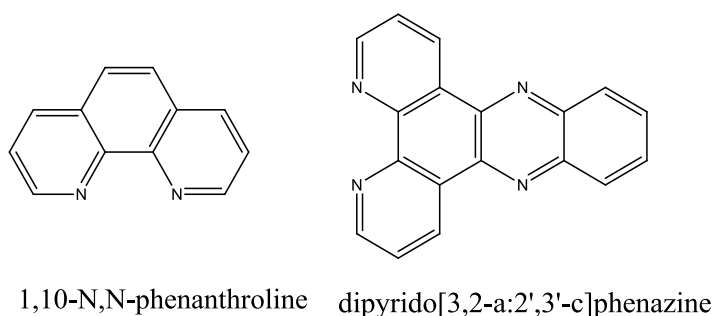


Fig 2.6 structure 1,10-N,N-phenanthroline (phen) and dipyrido[3,2-a:2',3'-c]phenazine (dppz)

The octahedral coordination geometry of the Ru (II) ion enables two potential configurations, the left-handed ( $\Delta$ ) and right-handed ( $\Lambda$ ) “propeller-like” structure (Fig 2.7), which are non-superimposable mirror image of each other, i.e. they are chiral.

In the earlier studies of ruthenium complexes with DNA,  $[\text{Ru}(\text{phen})_3]^{2+}$  was investigated, and intercalation was suggested as the main binding mode of the ruthenium complexes[29-30]. DNA binding geometry is slightly different between the  $\Delta$ -form and  $\Lambda$ -form of the complexes, as they are adapted to the different chiral DNA binding sites [29, 31-32]. The complex  $[\text{Ru}(\text{phen})_2\text{dppz}]^{2+}$ (Fig 2.8c) was made up by extending one phen (Fig 2.8d) to a dppz unit, and this complex has been studied intensively as it has very interesting photophysical and diverse DNA binding properties [33-35].

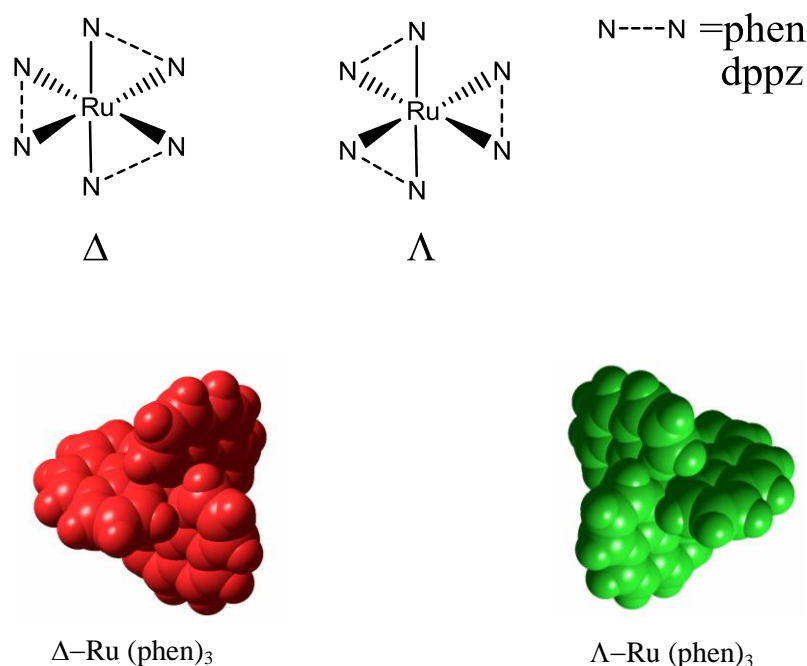


Fig 2.7 left-handed and right-handed propeller-like structures

The nitrogens in the middle ring of the dppz ligand are strongly affected by hydrogen bonding, which plays a significant role in the decay of the excited state in polarized solvent, *e.g.* water. The dppz ligand of  $[\text{Ru}(\text{phen})_2\text{dppz}]^{2+}$  binds into the DNA by intercalation between the base pairs. Upon intercalation, the dppz-ligand is embedded in an organic environment, which means that the nitrogens are protected from water, and then the emission quantum yield of the complexes when bound to DNA is increased by several orders of magnitude ( $>10^3$ ), which is called “light-switch” effect [34, 36]. This increase of emission prompts the fluorescence measurement a useful tool for studying the interaction between  $[\text{Ru}(\text{phen})_2\text{dppz}]^{2+}$  and DNA. The  $\Delta$  enantiomer of  $[\text{Ru}(\text{phen})_2\text{dppz}]^{2+}$  reveals a far higher emission intensity than the  $\Lambda$  enantiomer, in spite of only a slightly different DNA binding geometry existed for those two enantiomers[34].

Prior to this work, by accident,  $\Delta,\Delta$ - $[\mu\text{-(bidppz)(phen)}_4\text{Ru}_2]^{4+}$  P (Fig 2.8b) and ct-DNA was kept in room temperature for two weeks and it was revealed that the complexes were rearranged to an intercalated mode of binding with strong fluorescence [37] and lots of investigations have been undergoing following this discovery[38-41]. A new binuclear complex  $[\mu\text{-(bidppz acetylene)(phen)}_4\text{Ru}_2]^{4+}$  PA (Fig 2.8a) and its two enantiomers were investigated in this thesis.

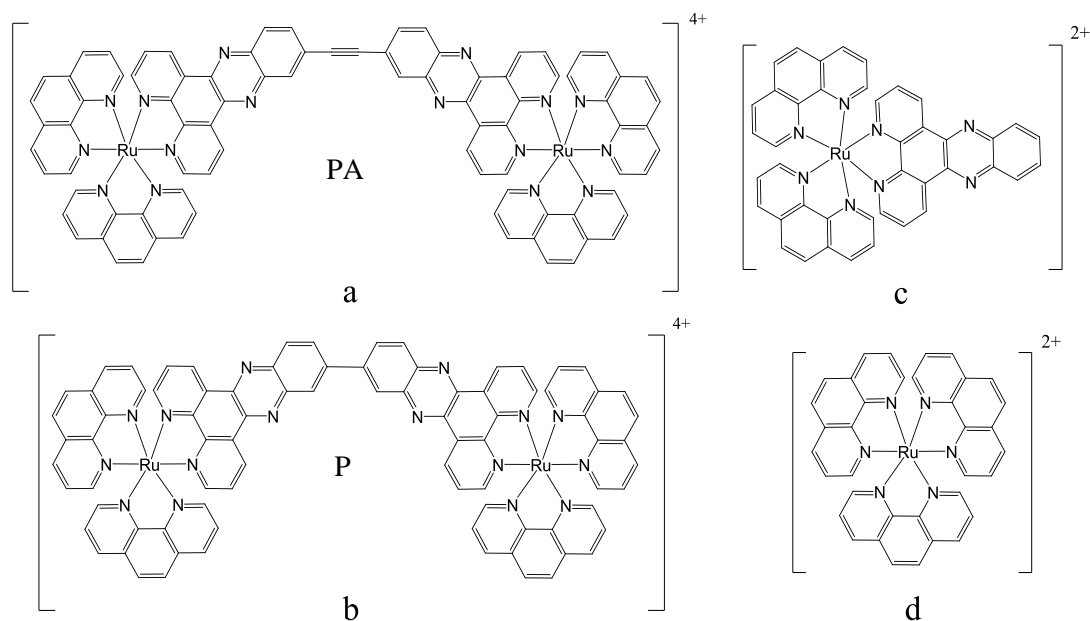


Fig 2.8 structures of ruthenium complexes: Binuclear intercalators a:  $[\mu\text{-(bidppz acetylene)(phen)}_4\text{Ru}_2]^{4+}$ ; b:  $[\mu\text{-(bidppz)(phen)}_4\text{Ru}_2]^{4+}$ ; single nuclear intercalators; c:  $[\text{dppz(phen)}_2\text{Ru}]^{2+}$ ; d:  $[(\text{phen})_3\text{Ru}]^{2+}$

The complex PA investigated in this thesis work is a new structure (Fig 2.8a) compared with the complexes studied before. The structure of PA shows a longer linkage bond, acetylene, between two monomer  $[\text{Ru(phen)}_2\text{dppz}]^{2+}$  halves than the old investigated complex P.

## 2.4 Spectroscopy

Light is a type of electromagnetic radiation and hence consists of an electrical field and a magnetic field. The interaction between a molecule and photons is the base of all spectroscopic phenomena. Absorption is the process when the energy of a photon is transferred to the sample of interest, resulting in electronic excitation of the molecules in the sample[42]. The light can only be absorbed by the sample in a certain wavelength with the corresponding energy gap between the states (Eq.1):

$$\Delta E = E_1 - E_2 = \hbar\nu = hc/\lambda \quad \text{Eq.1}$$

Where  $\nu$  is the frequency of radiation,  $\lambda$  is the wavelength of radiation,  $h$  is the Plank constant and  $c$  is the speed of light.

The possibilities of the electronic transitions in a molecule are often depicted in a Jablonski diagram (Fig 2.9). A transition between two different electronic energy levels can be induced by the energy supplied by photons, and the electron will “jump”

from the relative low energy ground singlet state ( $S_0$ ) to high energy level excited singlet state ( $S_n$ ). During the process the photons will be destroyed. Finally, the absorbed energy will be released in the form of radiation energy or thermal energy. Very rapidly the energy will be relaxed from the higher excited state  $S_n$  to the first excited energy state  $S_1$  by internal conversion and vibrational relaxation. Here are three main pathways for the energy relaxation from the first excited state ( $S_1$ ) to the ground state ( $S_0$ ): non-radiative internal conversion to  $S_0$ , emission of photons by fluorescence (F) to  $S_0$  or non-radiative intersystem crossing to the first triplet state ( $T_1$ ) from where relaxation to  $S_0$  can occur by non-radiative processes or by emission photons by phosphorescence (P). The emission from ruthenium complexes in this study is formally phosphorescence since the excited state is a triplet, however, due to spin-orbit coupling at the heavy ruthenium atom, these processes are much faster than ordinary phosphorescence and will thus be termed “fluorescence” in this study.

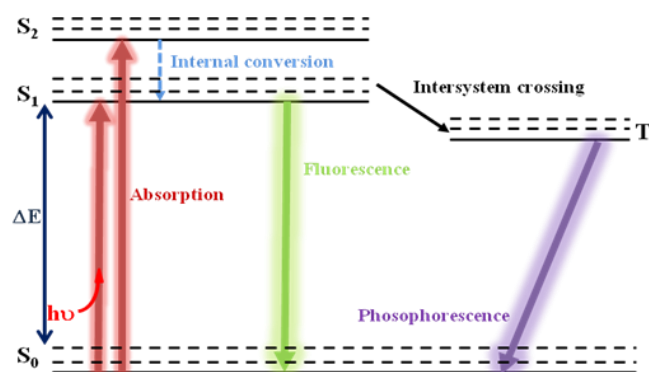


Fig 2.9 Jablonski diagram

### 2.4.1 Absorption and Fluorescence

Light absorption and emission are the most common methods to study molecules and interactions between molecules (Fig 2.11). In the absorption measurement, the samples of interest are illuminated by light of a defined wavelength and the light intensities before and after passing through the sample are measured:

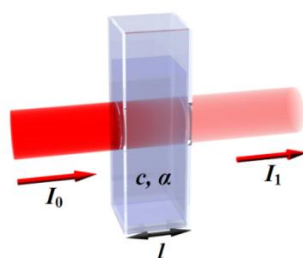


Fig 2.10 the process of absorption[43]

$$A(\lambda) = -\log_{10} \left( \frac{I_1}{I_0} \right) = \varepsilon(\lambda) \cdot c \cdot l \quad \text{Eq.2}$$

Where  $A(\lambda)$  is the absorbance at the wavelength  $\lambda$ ,  $I$  is the intensity of the output of light,  $I_0$  is the intensity of the input of light,  $\varepsilon$  is the extinction coefficient ( $\text{M}^{-1}\text{cm}^{-1}$ ),  $c$  is the concentration of the sample (M), and the  $l$  is length of the light pathway (cm). Absorbance of a sample is the logarithmic ratio of incident and transmitted light, and the concentration of sample can be calculated by Beer- Lambert's law (Eq.2).

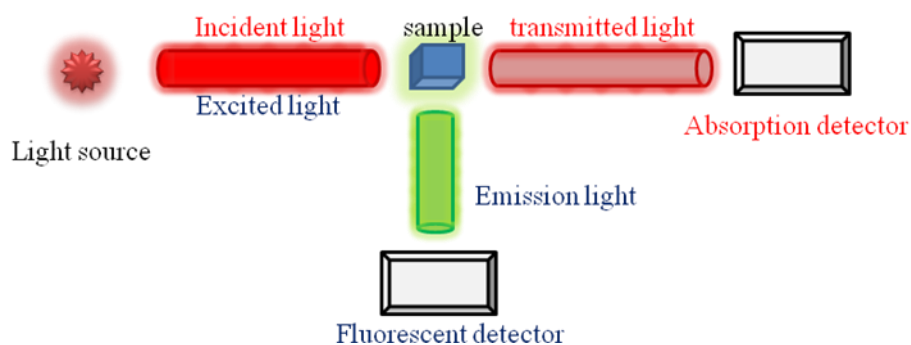


Fig 2.11 Setup of absorption and emission measurement

Fluorescence is a very convenient and sensitive method to study fluorescent molecules and their interactions with other molecules. Fluorescence efficiency is usually referred to as the fluorescence quantum yield ( $\Phi$ ) and can be calculated as:

$$\Phi = k_F / (k_F + k_{IC} + k_Q[Q]) \quad \text{Eq.3}$$

Where  $k_F$  is the rate constant for fluorescence and  $k_{IC}$  is the rate constant for internal conversion.  $k_Q$  is the rate constant for collisional quenching and  $[Q]$  is the concentration of the quencher.

The time constant for the decay of the excited state, called the emission lifetime ( $\tau$ ), is an important parameter for the phenomena, Eq.4. The measurement process of the lifetime will be explained in the following part.

$$\Phi = k_F / (k_F + k_{IC} + k_Q[Q]) \quad \text{Eq.4}$$

#### 2.4.2 Time-Domain Lifetime Measurement

Time-domain lifetime measurements is widely used in fluorescence spectroscopy (Fig 2.12 right), particularly in bio-macromolecules.[44] During the measurement, the sample is excited with a short pulse of light (Fig 2.12 left). The width of the pulse is

preferably much shorter than the decay time  $\tau$  of the sample molecules. The time-dependent fluorescent intensity is measured following the excitation pulse, and the decay time  $\tau$  can be calculated from the slope of a plot of  $\log I(t)$  versus  $t$  (Eq.5), or from the time at which the intensity decreases to  $1/e$  of the intensity at  $t = 0$  [45].

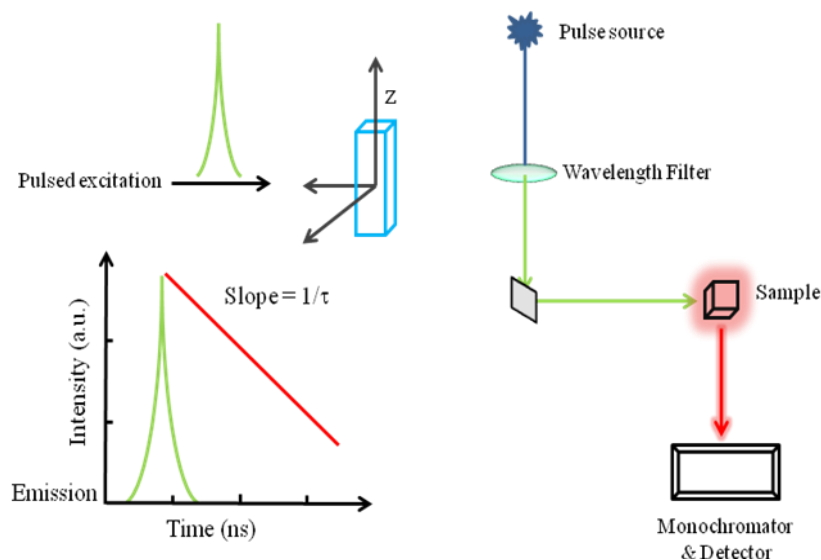


Fig 2.12 Pulse or time-domain measurement and setup of lifetime measurement (green curve in spectra is the intensity versus time and red line is the logarithmic intensity versus time)

$$I(t) = I_0 e^{-t/\tau} \quad \text{Eq.5}$$

$$t = -\tau(\ln I_t - \ln I_0) \quad \text{Eq.6}$$

Where  $I(t)$  is the fluorescent intensity at time  $t$ ,  $I_0$  is the intensity of incident pulse and  $\tau$  is the lifetime of the sample.

In this work, the ruthenium complex binds the DNA by electrostatic interaction immediately after mixing, and in this state, no emission can be observed due to quenching by hydrogen bonding solvent molecules [34, 36]. Then with time, electrostatic interaction turns into intercalation mode with a strong fluorescence which can be easily measured. Different binding environment of each complex molecule will vary the lifetime of emission. In this condition intensity decay will follow to a multi-exponential model:

$$I(t) = \sum_i \alpha_i e^{-t/\tau} \quad \text{Eq.7}$$

In this expression the  $\alpha_i$  values are called the pre-exponential factors which represent the relative fraction of the different lifetimes. For ruthenium dppz-complexes DNA, binding to DNA, a bi-exponential model is often sufficient:

$$I(t) = \alpha_1 e^{-t/\tau_1} + \alpha_2 e^{-t/\tau_2} \quad \text{Eq.8}$$

$$\tau_{average} = \alpha_1 \tau_1 + \alpha_2 \tau_2 / (\alpha_1 + \alpha_2) \quad \text{Eq.9}$$

## 2.5 Polarized Spectroscopy

Polarized spectroscopy is based on polarized light and is a very effective technique to acquire information about the interaction between molecules, as well as orientation and configuration of the molecules. Polarization is a property of the light that describes the orientation of the oscillations of the electric field. Light can be linearly polarized where the electric field of the light beam oscillates in a same plane, and also left-handed or right handed circularly polarized in where the oscillations occur in a helical mode. Linear dichroism and circular dichroism are most common techniques based on these two types of polarization of light in practical application.

### 2.5.1 Linear Dichroism

Linear dichroism, LD, is a spectroscopic technique that is primarily used to study the functionality and structures of molecules. The difference in absorption of light polarized parallel and perpendicular to an orientation axis give the signal of LD (Fig 2.13)[42]. The LD of an oriented molecule can be calculated using the following equation:

$$LD(\lambda) = A_{\parallel}(\lambda) - A_{\perp}(\lambda) \quad \text{Eq.10}$$

In order to measure an LD signal, a sample with oriented molecules is necessary. Orientation can be achieved, for example, in an electric field or by stretching a polymer matrix containing the molecule of interest. Large molecules, such as DNA, can be orientated by a flow gradient (Fig 2.14). The sample solution of interest is placed in the narrow gap between two cylinders of a Couette cell, one of which is rotated creating a shear gradient that aligns the DNA. Flow-LD is an established method to determine binding of small molecules to DNA and has recently been shown to also work excellently for DNA binding-proteins[46].

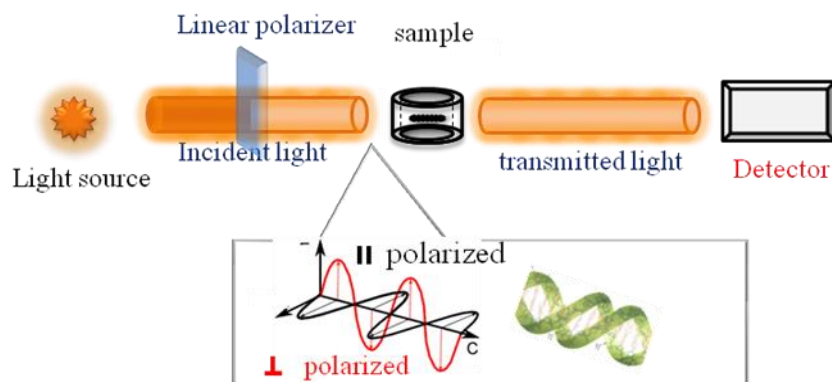


Fig 2.13 setup of LD spectropolarimeter and linear polarized light

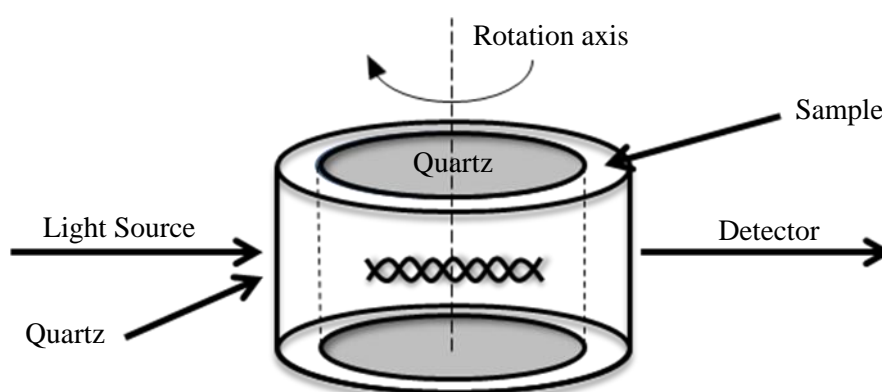


Fig 2.14 The principle of flow-LD of DNA in a Couette cell

The reduced linear dichroism  $LD^r$  is a dimensionless quantity that only depends on the geometric arrangement of the molecular transition moments relative the macroscopic orientation. It is obtained by dividing the linear dichroism for a given sample and pathlength by the corresponding isotropic absorption, and is wavelength independent for a purely polarized transition.

$$LD^r = \frac{(A_{\parallel} - A_{\perp})}{A_{iso}} = \frac{LD}{A_{iso}} = 3 \cdot S \cdot O = 3 \cdot S \cdot \left( \frac{3\cos^2\alpha - 1}{2} \right) \quad \text{Eq.11}$$

Where  $S$  ( $0 \leq S \leq 1$ ) is the orientation parameter which is the degree of orientation in the sample;  $S=1$  for a perfectly orientated sample and  $S=0$  for an isotropic sample;  $O$  is the optical factor;  $\alpha$  is the angle between the macroscopic orientation axis and the transition moments of small molecules. Also,  $LD^r$  can be interpreted as the product of the orientation factor  $S$  and the optical factor  $O$ . The macroscopic level of alignment is expressed by the orientation factor  $S$ . For a DNA sample (Fig 2.15), the  $S$  value can be calculated by assuming  $\alpha$  to be  $86^\circ$  in the absorbance band at 260nm, but this assumption may be invalid for overlapping absorption bands[47].

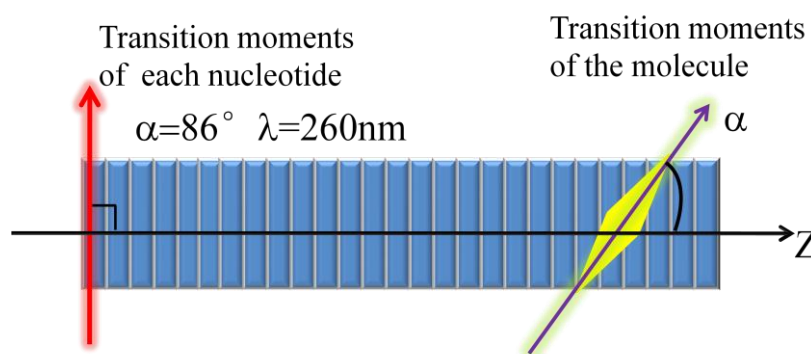


Fig 2.15 interpretation of optical factor and angle  $\alpha$  in DNA sample[47]

### 2.5.2 Circular Dichroism

Circular dichroism CD is probing changes of polarization of the light transmitted by a sample containing chiral molecules[42]. At the heart of the instrument is the polarizer that enables one to tune and change the light polarization, before it hits the sample chamber (Fig 2.16). The polarization of light is defined by the direction of its electric field and magnetic field vectors.

$$CD = \Delta A = A_L - A_R = \Delta \epsilon \cdot c \cdot l \quad \text{Eq.12}$$

Where,  $\Delta A$  is the difference between absorbance of the left and right circularly polarized light;  $A_L$  is the absorbance of left-handed circularly polarized light and  $A_R$  is the absorbance of right-handed circularly polarized light.  $\Delta \epsilon$  is the difference between two different extinction coefficients of right and left polarized light.

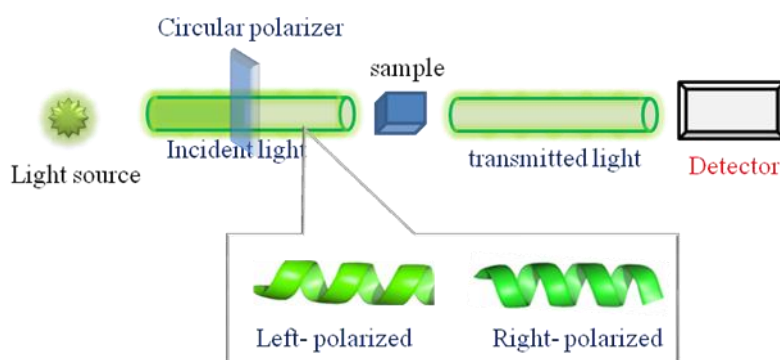


Fig 2.16 setup of CD spectropolarimeter and circularly polarized light

### 2.6 Kinetics of Chemical Reactions

Reaction kinetics is one of the most essential parts in physical chemistry research. Chemical kinetics is the study of the rate of a chemical process and is affected by the different reaction conditions. Thermodynamic equilibrium can be fairly rapidly established between reactant and product with a preferable condition for the reaction.

The relative yield of product will be judged by the free energy. The decrease in free energy appears when a product is formed. One or more energy barrier must be overcome when the reaction proceeds (Fig 2.17). An empirical equation was observed from many reactions by Svante Arrhenius [48] more than hundred years ago. (Eq.13)

$$\ln k = \ln A - \frac{E_a}{RT} \quad \text{Eq.13}$$

Where the  $E_a$  is the activation energy which represents the critical energy possessed by reactant to promote the reaction occurring;  $A$  is a given value called pre-exponential factor,  $R$  is the ideal gas constant,  $T$  is Kelvin temperature and  $k$  is the rate constant.

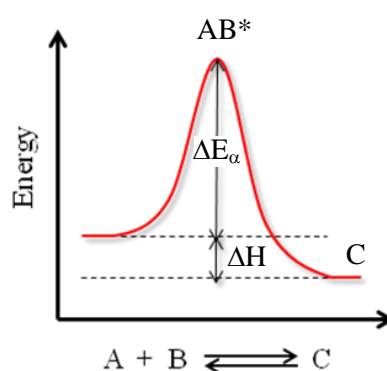


Fig 2.17 energy relation in a reaction

The process of the reaction in this thesis work can be depicted as:

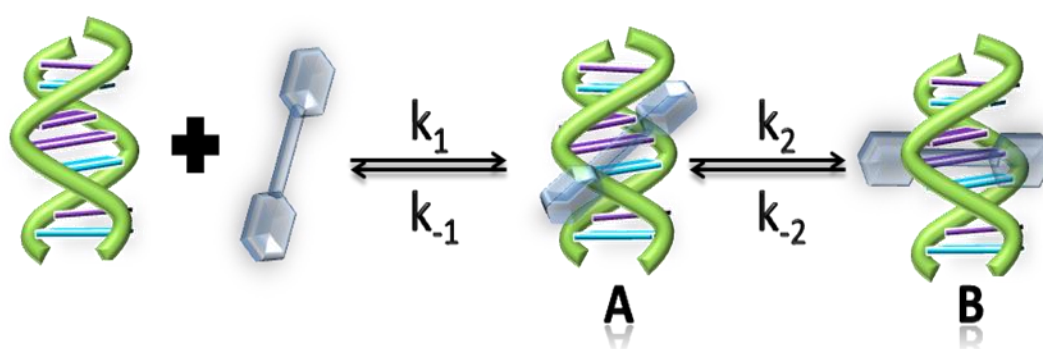


Fig 2.18 reaction process

Where  $A$  is the electrostatic interaction state of the complex with DNA and  $B$  is the threaded intercalation state,  $k_i$  is the rate constant of this reaction in each step. The process of threading goes slowly to equilibrium due to the high energy barrier of threading and unthreading steps.

Assuming that the first step of the reaction is fast enough, it can be ignored during the kinetic measurement, and all the starting materials, DNA and complex molecules, is found in state A at the beginning of the experiment. As we know, fluorescence can be measured only in intercalation state; therefore, the model can be simplified by fluorescence intensity measurement. The first-order of reaction model can be used to study the reaction process:

$$-\frac{d[A]}{dt} = k_2[A] \quad \text{Eq.14}$$

For coupled first-order reactions the emission intensity signal S can be expressed by a sum of exponentials, where the apparent rate constants are more or less complicated functions of the microscopic ones:

$$S(t) = \alpha_0 + \alpha_1 \cdot e^{k_1 \cdot t} + \alpha_2 \cdot e^{k_2 \cdot t} \quad \text{Eq.15}$$



### 3. Material and Methods

In this section, the materials and methods used will be briefly introduced.

#### 3.1 Sample preparation

##### 3.1.1 Buffer

The present work has been performed in 1mM Dimethylarsinic acid salt (KACK) buffer pH=7, with different concentration of NaCl. 150mM sodium chloride with 1mM KACK, was investigated initially in the thesis, but 50mM sodium chloride and 1mM KACK was then used as the buffer for the work.

##### 3.1.2 Ruthenium complexes

The synthesis of the two enantiomers of the new ruthenium complex PA follows the procedure described in [38], with tetraamino tolane, kindly provided by Johan Johansson, replacing tetraamino fluorene. The ruthenium complexes P were provided by Johanna Andersson. Stock solutions were made by dissolving a few crystals in sodium chloride buffer and stored at +5 °C. All the concentration of stock solution ranged from 0.8 to 1.2 mM. Concentrations were estimated through absorption measurements by Eq.2. Extinction coefficient used:  $\epsilon_{260nm}=200,000 \text{ M}^{-1} \text{ cm}^{-1}$  for **P** and **PA**.

##### 3.1.3 DNA

Calf thymus DNA and Poly (dA-dT)<sub>2</sub> were purchased from Sigma-Aldrich, both as a sodium salt. Stock solutions were prepared by dissolving the salt in sodium chloride buffer with slight stirring over night. The solution of stock ct-DNA were filtered (filter pore size 0.7 μM) twice afterwards to separate DNA from amounts of light-scattering contaminations and then store in a freezer at -20 °C. DNA stock solutions were diluted in sodium chloride buffer to samples of concentrations just 240 μM to be used for equal amount mixing with ruthenium complex in experiments. Diluted DNA solution were stored in +5 °C and considered expired if not used within three weeks; the same for the solution of ruthenium complexes.

##### 3.1.4 Mixing

In the experiments described in the report, solutions were equal amount mixed to reach the final concentrations 120 μM and 6 μM of DNA and ruthenium complexes, respectively. This corresponds to 16 base pairs per ruthenium dimer. 3 weight % of sodium dodecyle sulphate stock solution (SDS) was added into the final binding states solutions for dissociation reaction with the final concentration of 0.6 weight % SDS in the mixture. The binding process between different complexes and DNA have

revealed to be very slow for some mixtures, while relatively fast for the other. The samples heated at 50 C° after 15 hours can be considered to have reached the final binding mode.

### 3.2 Absorption

Absorption measurements were primarily used to estimate the concentration of solutions used in the different experiments, but also to create absorption spectra of the final binding states. All were performed on either a Cary 4000 UV-Vis spectrophotometer (Varian, USA) or Cary 5000 UV-Vis spectrophotometer (Varian, USA), at room temperature and corrected with a pure buffer baseline.

### 3.3 Linear Dichroism

LD experiments were performed on a Chirascan LD spectrophotometer (Applied Photophysics, UK). The DNA sample was oriented in a Couette cell as described earlier. Rotation was set at 1000 rpm. Directly after each measurement, a baseline was created by recording a spectrum without rotation.

### 3.4 Fluorescence

Fluorescence techniques were used to record emission and excitation spectra of the final binding state as well as for the measurement of association and dissociation kinetics. The steady state fluorescence and the time-based were both performed on the Cary Eclipse Fluorescence Spectrophotometer (Varian, USA). Emission spectra were collected between 450 to 800 nm using an excitation wavelength of 405nm. For the kinetic measurements an excitation wavelength of 405nm and emission wavelength of 630 nm were used. For the association experiments, temperature-equilibrated solutions of DNA and ruthenium complex were mixed directly in the cuvette and data collection obtained was started within a few seconds. The dissociation experiments were started by mixing final binding state samples and SDS. Experiments were started immediately after mixing for the purpose of minimizing the loss of data in the early duration.

### 3.5 Fluorescence Lifetime Measurement

Nanosecond emission decays for the mixture samples were performed on an Nd:YAG laser (Coutinnum Surelite II-10, pulse width < 7 ns, CA). The excited light of defined wavelength is at 355 nm, and the emission light was detected after crossing over the monochromator at 630 nm and filtered by a Hamamatsu R928 photomultiplier tube with perpendicular angle of excited light. The signals of decays were collected by a 200 MHz digital oscilloscope (Tetronix TDS2200 2Gs/s) and saved by Lab View-program. During the experiment different time windows were

used for measurements (25ns, 100ns, 250ns, 500ns, 1  $\mu$ s) with different energy of the pulse light.

### **3.6 Analysis of Kinetics Data and Decay Time**

Data acquired in the kinetic studies and fluorescence lifetime measurements was analysed in MATLAB software (Mathworks, Inc.) by using the minimization *nexfit* program to simulate the exponential traces.



## 4. Results and Discussions

The results and discussion of the thesis are presented in this section.

### 4.1 Experiment Conditions

In the earlier studies of ruthenium complex P, experimental conditions was mentioned that the maximum ratio between complex and DNA base pairs is 1 complex per 8 base pairs in 150 mM sodium chloride buffer. Due to a higher hydrophobicity, complex PA easily precipitates in 150mM sodium chloride buffer at a certain maximum ratio (1complex per 8 base pairs) between the complex and DNA base pairs. It was a key issue for us to find better experimental conditions for PA. A series ratio between PA and DNA base pairs was investigated (from minimum 1 complex per 150 base pairs to 1 complex per 10 base pairs) in different conditions (MQ-water, 50 mM NaCl buffer and 150 mM NaCl buffer) by absorption and LD to circumvent the precipitation, respectively. 50 mM NaCl buffer was used for this thesis.

### 4.2 Absorption

In the studies of the interaction between PA and DNA, determining the binding mode is naturally, one of the main purposes of this thesis. In the earlier study of P, threading intercalation is considered as the final binding mode [38, 41, 49]. Fig 4.1 shows the absorption spectra of the four complexes free in solution and when bound to ct-DNA before and after heating. The DNA bases exhibit  $\pi \rightarrow \pi^*$  UV-Vis transitions in the 240 to 275 nm region (with  $\epsilon_{260} = 6600$  per base)[50]. Intra-ligand phen transition peak is still around 260nm, which will strongly cover the DNA absorption ( $\epsilon = 200,000$ ). P shows a peak at 320nm, which is a  $\pi \rightarrow \pi^*$  long axis transition in the bidppz bridge, but for the PA, the corresponding peak of the bidppz acetylene bridge is broad and a little blue shifted to approximately 300 nm. The alteration of the  $\pi \rightarrow \pi^*$  long axis transition may arise from rotation of the acetylene bridge between the two monomers units. The peak between 400 and 500 nm is a broad band of  $d \rightarrow \pi^*$  metal-to-ligand charge transfer (MLCT) transitions overlapped with a band arising from the phenanthroline ligands, and the band in this visible region causes the red-orange color of the complex.

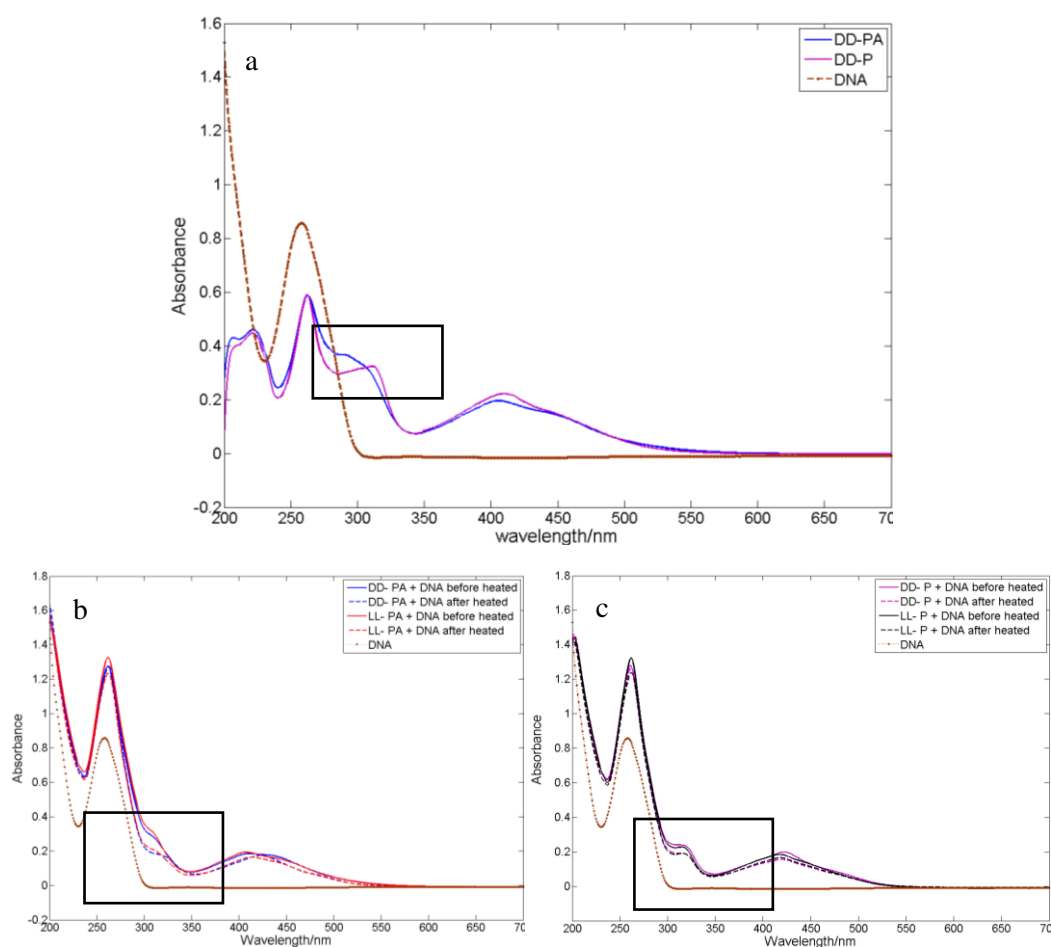


Fig 4.1: a: the absorption spectrums of b: The absorption spectrum of pure ct-DNA, P and PA mixed with DNA before heated (line) and after heating (dash line) at 50 °C over night.

The peaks at 260 nm decreases when the complexes binds to DNA, and this decrease is considered that the DNA bases was bound to complexes which was affected by the intra-ligand transition of phen. The broad band around 320 nm, which arises from the  $\pi \rightarrow \pi^*$  long axis transition in the bidppz bridge, becomes weaker after intercalation because of interactions with the DNA bases. For the MLCT transition region around 400 to 500 nm, a hypochromicity was observed after mixing with DNA, which has been reported before[34].

### 4.3 Circular Dichroism

Fig 4.2 shows the CD spectrum of the different enantiomers of P and PA. After the complexes binding with ct-DNA, the negative peaks around 400 to 500 nm are disappeared for  $\Delta, \Delta$ -PA while that of  $\Lambda, \Lambda$ -PA is not altered, and at 270 nm the negative peak of  $\Delta, \Delta$ -complexes and positive peak of  $\Lambda, \Lambda$ -complexes are both increased. The same changes of CD spectrum also can be observed from poly(dAdT)<sub>2</sub> DNA bound to complexes.

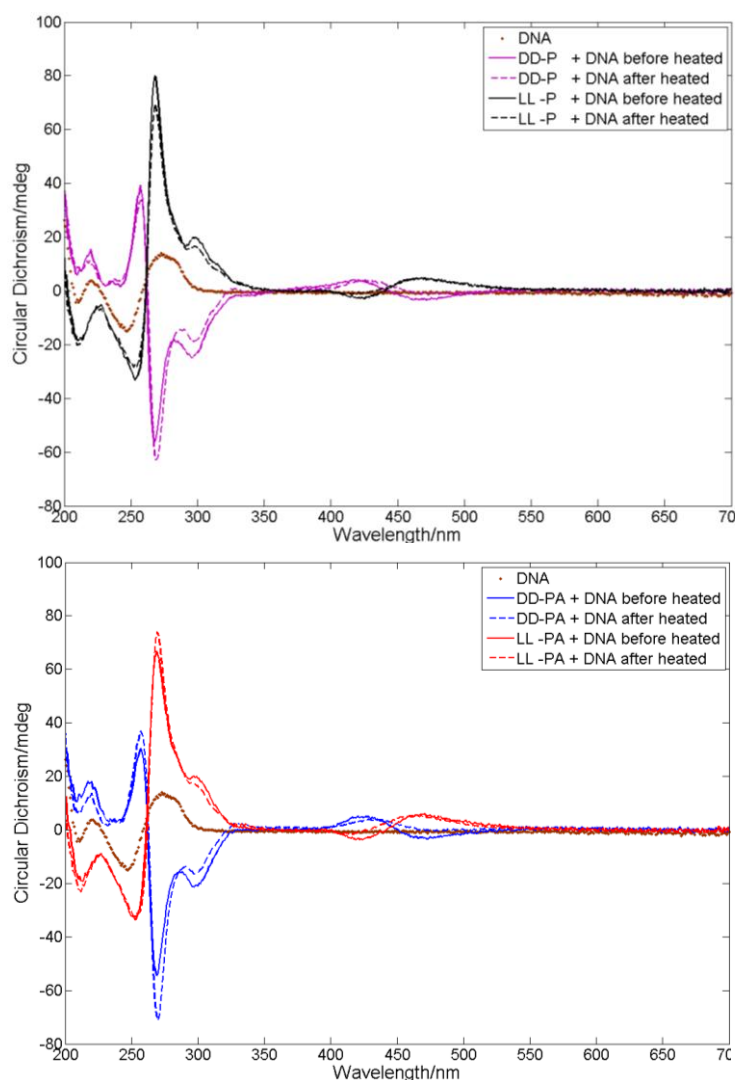


Fig 4.2 the CD spectrum of four complex and complexes binding with DNA; top: the CD spectrum of P before and after heated at 50 °C; bottom: the CD spectrum of PA before and after heated at 50 °C

#### 4.4 Linear Dichroism

Flow LD is an effective way to investigate the binding mode of the complex with DNA. Fig 4.3 shows the LD spectra of the complexes bound to DNA after incubation at 50 °C for 24 hours. As described in prior work, a decreased negative signal of the phenanthroline ligand at 260 nm and an increased negative signal of the long axis transition of the bidppz bridge at 320 nm are associated with the complex binding to DNA[40]. The amplitude of the LD signals at constant concentration is dependent on the binding geometry between the complex and DNA strands, and as the binding mode of the dimer changes from groove binding or electrostatic interaction in the beginning to the final threading intercalation mode the LD signal changes. In the visible region of the LD spectrum, the complexes of  $\Delta,\Delta$ - and  $\Lambda,\Lambda$ -P and  $\Delta,\Delta$ -PA

show similar patterns after binding with DNA. We can suppose that they have the same binding geometry when bound to ct-DNA. The crucial matter of proposing the binding mode is the bidppz bridge signal.  $\Delta$ ,  $\Delta$ -P and  $\Lambda$ ,  $\Lambda$ -P both express a decrease signal and increase signal for the phenanthroline ligand and bidppz bridge, respectively.

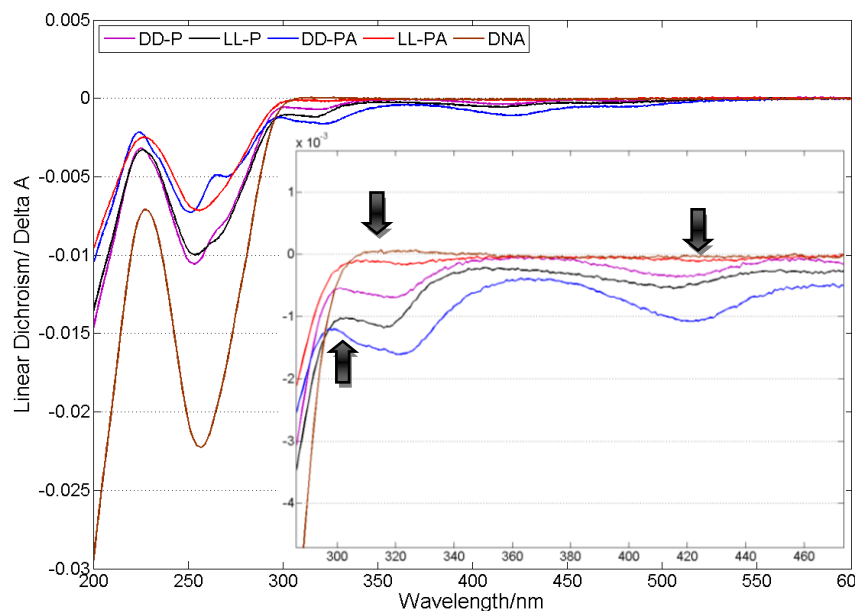


Fig 4.3 the spectrum of pure DNA sample and  $\Delta$ ,  $\Delta$ -P,  $\Lambda$ ,  $\Lambda$ -P,  $\Delta$ ,  $\Delta$ -PA and  $\Lambda$ ,  $\Lambda$ -PA mixed with equal volume DNA sample and heated at 50 °C for 24hours. 200 to 450 nm region is zoomed up.

For the PA complexes, only  $\Delta$ ,  $\Delta$ -PA show the variety of the signal while the  $\Lambda$ ,  $\Lambda$ -PA did not change the pattern so much compared with the DNA signal. In the 260 to 320 nm region, the LD signals changes with the binding of the complexes to DNA, which would be resulted from altering the DNA orientation. In the region between 300 to 500 nm, LD shows the signal of complexes bound to DNA. From the spectrum we can find that  $\Delta$ ,  $\Delta$ -P,  $\Lambda$ ,  $\Lambda$ -P and  $\Delta$ ,  $\Delta$ -PA show signals as the complexes bound to DNA. As the prior work, the signal in this region is the characteristic signal for binuclear ruthenium complexes bind to DNA[37], and  $\Delta$ ,  $\Delta$ -P and  $\Lambda$ ,  $\Lambda$ -P bind to DNA with threading intercalation.  $\Lambda$ ,  $\Lambda$ -PA shows no observable signal around 320 to 500 nm, and a reduced the signal at 260 nm, which indicate supposed that the  $\Lambda$ ,  $\Lambda$ -PA does not bind to DNA with threading intercalation or groove binding, just by disorder electrostatic interaction which decrease the orientation of DNA.

#### 4.5 Reduced Linear Dichroism

The reduced LD spectra calculated by the Eq.11 are shown in Fig 4.4. reduced LD can be used to calculate the angle between complex transition moment and DNA molecular orientation. For a simple assumption for acquiring the orientation factor  $S$ , the nucleobases in the DNA molecule is a good reference to calculate the  $S$  factor. Thus, the orientation factor of DNA is changed after being bound by a complex; the angles  $\alpha$  cannot be exactly calculated. The nucleobases are close to perpendicular to the ct-DNA molecular axis, which is  $\alpha=86^\circ$  [47]. Hence, the angle between the ct-DNA axis and complex transition moment can be calculated. The reduced LD of strongly negative signal at 320nm in P arising from the bidppz bridge transition moment can prove that the complex geometry in two-fold axis is approximately  $65^\circ$  to the DNA helix axis for both enantiomers [38, 51]. For  $\Delta,\Delta$ -PA, the reduced LD value is more negative than in the DNA base region at 260 nm, indicating that the binding ligand must be closer to  $90^\circ$  to the helix axis. Due to the overlapped by the positive MLCT band on the low energy around 400 to 450 nm, the exact reduced LD value and the angle cannot be determined. The UV region around 250 nm of reduced LD is an important part to investigate DNA sample orientation alternation after intercalated by complexes. For the pure DNA sample the reduced LD value around 250 nm is over -0.2, with the more complexes threading intercalated into DNA strands, a large decrease will be observed in this region.

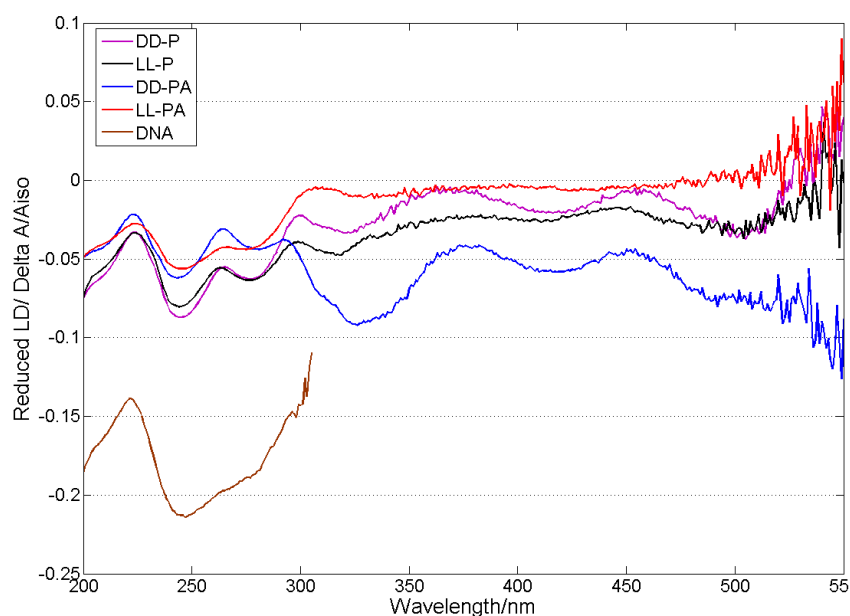


Fig 4.4 the reduced LD spectrum for DNA sample (brown) and DNA mixture with  $\Delta,\Delta$ -P (pink) and  $\Delta,\Delta$ -PA (blue)

Because the poly (dAdT)<sub>2</sub>-DNA was too short to obtain sufficient orientation of the sample in the LD measurements. Therefore, binding mode of complexes with poly (dAdT)<sub>2</sub>-DNA cannot be investigated by LD.

#### 4.6 Fluorescence

After complexes intercalate into DNA, fluorescence was measured while the samples were excited at 405 nm, which is the wavelength for the maximum absorption in the visible region by the samples, which 405 nm are used to excite all the complexes. During the experiments, shifted the wavelength cannot alter the shape of emission spectrum only the maximum intensity, so the same excitation wavelength for both P and PA was used. Fig 4.5 shows the emission spectra for the complexes bound to ct-DNA and poly (dAdT)<sub>2</sub>-DNA. From the spectra of bound with ct-DNA and poly (dAdT)<sub>2</sub>-DNA, different intensity of each complex can be observed. Apparently, the complex bound with poly (dAdT)<sub>2</sub>-DNA shows a higher intensity than that with ct-DNA.

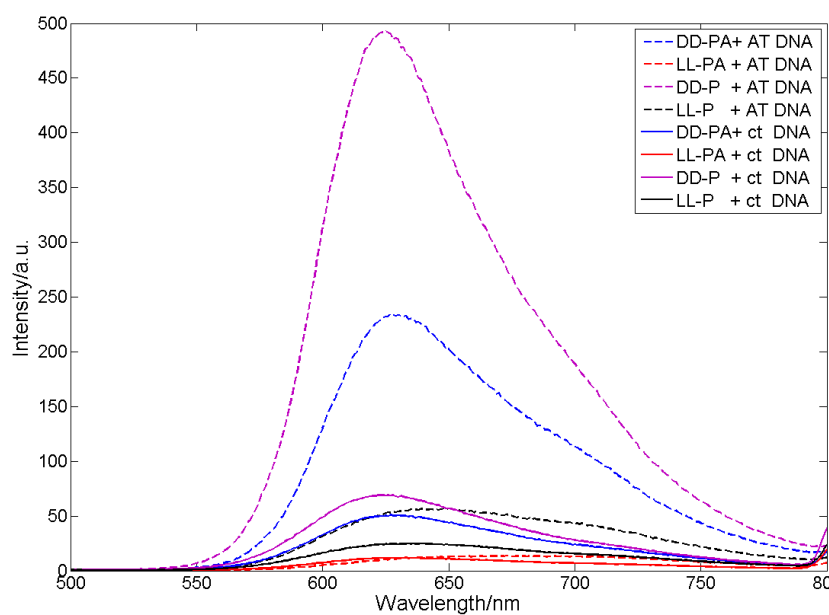


Fig4.5 the fluorescence spectrums of complexes interact with ct-DNA and poly (dAdT)<sub>2</sub> DNA, respectively: line- the four complexes react with ct-DNA after heated at 50 °C over night; dash line- the four complexes react with poly (dAdT)<sub>2</sub>-DNA after heated at 50 °C over night.

#### 4.7 Fluorescence Lifetime Measurement

The emission lifetime was measured on samples heated at 50 °C over night after mixing the complexes with ct-DNA. The intensity decays measured with 250 ns time window are used for analysis and the results are shown in table 2. Two lifetimes was used to fit the data for all four complexes. In the conditions used in this work, the

second lifetime, which dominate the steady state intensity, are slightly shorter for both enantiomers of PA than that for P.

	PA		P	
	$\Delta,\Delta$	$\Lambda,\Lambda$	$\Delta,\Delta$	$\Lambda,\Lambda$
$\tau_1(\alpha)/\text{ns}$	53.9(0.58)	47.5(0.85)	63.3(0.51)	70.4(0.57)
$\tau_2(\alpha)/\text{ns}$	218.4(0.42)	220.3(0.15)	288.8(0.49)	333.2(0.43)
Average $\tau/\text{ns}$	123.0	73.42	173.8	183.4

Table 2 the results of lifetime measurement with 1- and 2- exponential model

#### 4.8 Binding Mode Summary

Above all, the binding mode of only  $\Delta,\Delta$ -PA is seen as threading intercalation for new complex PA. A strong negative peak at 320 nm and positive peak at 260 nm were considered as the signal of threading intercalation. These 2 peaks were strong observed of  $\Delta,\Delta$ -PA than  $\Delta,\Delta$ -P and  $\Lambda,\Lambda$ -P in LD spectrum. Also, fluorescence spectra of  $\Delta,\Delta$ -PA shows the emission after both ct-DNA and poly (dAdT)<sub>2</sub> DNA bound with  $\Delta,\Delta$ -PA due to the light-switch effect.  $\Lambda,\Lambda$ -P also has LD signals because of non threading intercalation from the previous study[38]. But with  $\Lambda\Lambda$ -PA, there is not any observable evidence confirm the threading intercalation happened. Because of the shorter strand of poly (dAdT)<sub>2</sub> DNA than ct-DNA, LD cannot give a signal, which means the LD cannot supply any evidence to study the binding mode of poly (dAdT)<sub>2</sub> DNA with  $\Delta,\Delta$ -PA. However, a much stronger emission intensity measured of poly (dAdT)<sub>2</sub> DNA bound with  $\Delta,\Delta$ -PA compared with ct-DNA. Hence, it is assumed that threading intercalation with poly (dAdT)<sub>2</sub> DNA is more selective than ct-DNA and of  $\Delta,\Delta$ -PA.

Then we consider the reduced LD values, the strong negative peak at 260 nm of DNA shows a good stretched orientation of DNA helix. The band at 260 nm of complex is the intra-ligands of phen transition polarization, when the complexes added to DNA sample, the 2 peaks will be overlapped. The earlier study shows that the DNA was intercalated by complex, the orientation will get better, which can be observed in reduced LD[34]. But for  $\Delta,\Delta$ -PA, after threading intercalation the orientation of DNA gets worse. This should be further studied in the future.

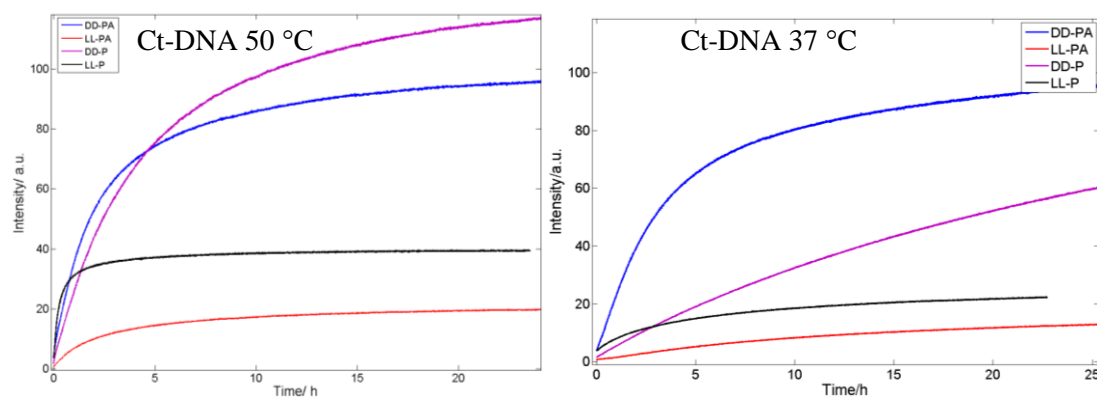
#### 4.9 Association Kinetic

The light switch effect can be used to measure the kinetics of the DNA-complex intercalation. The increase of quantum yield can be obtained due to the shielding of

the phenazine nitrogens, and it is a good way to quantify the degree of interaction. The experimental works concerning the kinetics of binding was performed on different interaction condition parameters. The condition parameters included: *complex*, *stereoisomer*, *type of DNA*, and *temperature*, where temperature is the main factor for the investigation of new complexes PA.

Much more attention was focused on the PA, the measurement of P enantiomers only are used as comparison between the PA and P association and dissociation process. The kinetics of P with ct-DNA is so slow at 25 °C that another temperature at 45 °C was used for comparison, but for poly (dAdT)<sub>2</sub>-DNA the reorganization kinetics is much faster for P.

Because  $\Lambda,\Lambda$ -PA shows very low intensity compared with  $\Delta,\Delta$ -P and included the result of LD, it is supposed that threading intercalation is not the binding mode of  $\Lambda,\Lambda$ -PA. The result can be observed from the plot, the  $\Lambda,\Lambda$ -PA is very low intensity of kinetics measurement. Hence, comparison of  $\Delta,\Delta$ -PA and  $\Delta,\Delta$ -P is the main point in this part. Data of the kinetics measurements were fitted to multi-exponential model described earlier. Generally, associations of both types of DNA and PA or P required two exponentials, but for dissociation one exponential is enough.



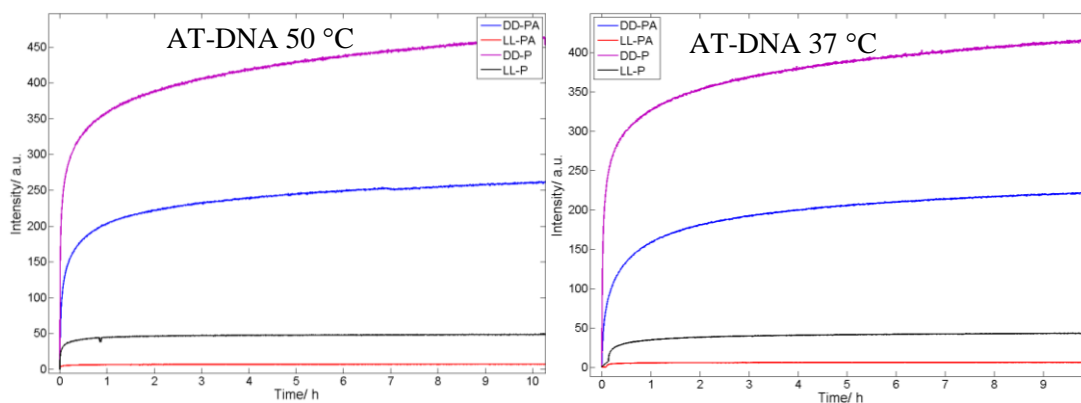


Fig 4.6 the time-based emission measurements at 37 and 50 °C with ct-DNA and poly (dAdT)<sub>2</sub> DNA

Fig 4.6 shows the association kinetics at different temperatures for P and PA and data of  $\Delta, \Delta$ -PA and  $\Delta, \Delta$ -P can be acquired from table 4. For the binding process at 50 °C, the order of the rate in first stage is:  $\Delta, \Delta$ -P >  $\Delta, \Delta$ -PA >  $\Delta, \Delta$ -P. In the second binding phase, the results are obvious from the plot:  $\Delta, \Delta$ -P >  $\Delta, \Delta$ -P >  $\Delta, \Delta$ -PA. Conclude the results in average rate, which contain the component of each step to the final emission. The average rate of two phases in order is:  $\Delta, \Delta$ -P >  $\Delta, \Delta$ -P >  $\Delta, \Delta$ -PA. In 37 °C, from Table 4, the order of the first stage rate constant for binding process is:  $\Delta, \Delta$ -P >  $\Delta, \Delta$ -PA >  $\Delta, \Delta$ -P, and the second step rate constants of complexes are so small that they are easy to differ from the plot. For average rate, the  $\Delta, \Delta$ -PA is the fastest process to binding to ct-DNA to equilibrium. The first step is considered as the process of threading intercalation, thus the first process is more interesting to compare. The data of all the complexes binding to DNA can be acquired at Appendix II.

T (°C)	$k \cdot 10^4 / s^{-1}$	$\Delta\Delta$ -PA	$\Delta\Delta$ -P
50	$k_1(\alpha_1)$	1.74(0.42)	1.15(0.63)
	$k_2(\alpha_2)$	0.28(0.58)	0.31(0.37)
	$k_{av}^*$	0.44	0.58
45	$k_1(\alpha_1)$	1.68(0.67)	0.78(0.33)
	$k_2(\alpha_2)$	0.32(0.33)	0.25(0.67)
	$k_{av}^*$	0.7	0.32
37	$k_1(\alpha_1)$	1.04(0.62)	0.61(0.05)
	$k_2(\alpha_2)$	0.15(0.38)	0.09(0.95)
	$k_{av}^*$	0.3	0.09

Table 4 the rate constants of ct-DNA bound by different compound in three different temperatures; \*  $k_{av}$  is calculated followed weighted average:  $k_1^* \alpha_1 + k_2^* \alpha_2$ , where the  $\alpha$  is the component of each rate constant to reach the final emission.

Table 5 is the data collection of kinetics of complexes binding to poly(dAdT)<sub>2</sub> DNA, the first rate constant of all compounds dominate the process to final emission. Thereafter, the first rate constants are used to compare the binding rate to poly(dAdT)<sub>2</sub> DNA. The rate order in 50 °C is: Δ,Δ-PA>Δ,Δ-P>Λ,Λ-P. In 37 °C, the order is: Δ,Δ-P>Δ,Δ-PA (Λ,Λ-P). It is nearly the same rate constant of Δ,Δ-PA and Λ,Λ-P in 37 °C. for the poly (dAdT)<sub>2</sub> DNA, the kinetics curves give a same pattern in 37 and 50 °C. From the data, the kinetically selectivity of P and PA are the same, which the poly (dAdT)<sub>2</sub> DNA is fast bound by the both P and PA.

T (°C)	$k \cdot 10^4 / s^{-1}$	ΔΔ-PA	ΔΔ-P	ΛΛ-P
50	$k_1(\alpha_1)$	15.9(0.73)	37(0.71)	13.2(0.85)
	$k_2(\alpha_2)$	0.9(0.27)	0.87(0.29)	0.69(0.15)
	$k_{av}^*$	2.9	2.8	3.5
37	$k_1(\alpha_1)$	5.2(0.63)	22.8(0.72)	8.42(0.72)
	$k_2(\alpha_2)$	0.26(0.37)	0.44(0.28)	0.46(0.28)
	$k_{av}^*$	0.54	3.79	1.28
25	$k_1(\alpha_1)$	12(0.55)	31.4(0.90)	9.2(0.73)
	$k_2(\alpha_2)$	0.88(0.45)	0.84(0.10)	0.72(0.27)
	$k_{av}^*$	2.1	2.79	2.1

Table 5 the rate constants of poly (dAdT)<sub>2</sub>-DNA bound by different compound in three different temperatures; \*  $k_{av}$  is calculated followed weighted average:  $k_1 \cdot \alpha_1 + k_2 \cdot \alpha_2$ , where the  $\alpha$  is the component of each rate constant to reach the final emission.

Fig 4.7 is the comparison of the binding process between Δ,Δ-PA and Δ,Δ-P in different temperatures with ct-DNA and poly (dAdT)<sub>2</sub> DNA. For ct-DNA, the rate constant of Δ,Δ-PA is less affected by temperature changes than that of Δ,Δ-P. The rate constant of Δ,Δ-PA is decrease from 0.44 to 0.3 with the temperature decrease between 50 to 37 °C. However, the rate constant of Δ,Δ-P is decrease from 0.58 to 0.09 with the temperature decrease in the same range.

The contrary results can be observed by bound to poly (dAdT)<sub>2</sub> DNA. The rate constant of Δ,Δ-PA is more affected by temperature changes, which is decrease from 2.9 to 2.1 with the range of 50 to 25 °C. For Δ,Δ-P, the rate constant varied from 3.79 to 2.79 with the temperature decreasing from 37 to 25 °C, which shows a similar rate between 50 °C and 37 °C from the plots.

The conclusion is that temperature shows larger impacts of the binding process with poly (dAdT)<sub>2</sub> DNA for Δ,Δ-PA than that with ct-DNA. An opposite result for Δ,Δ-P instead.

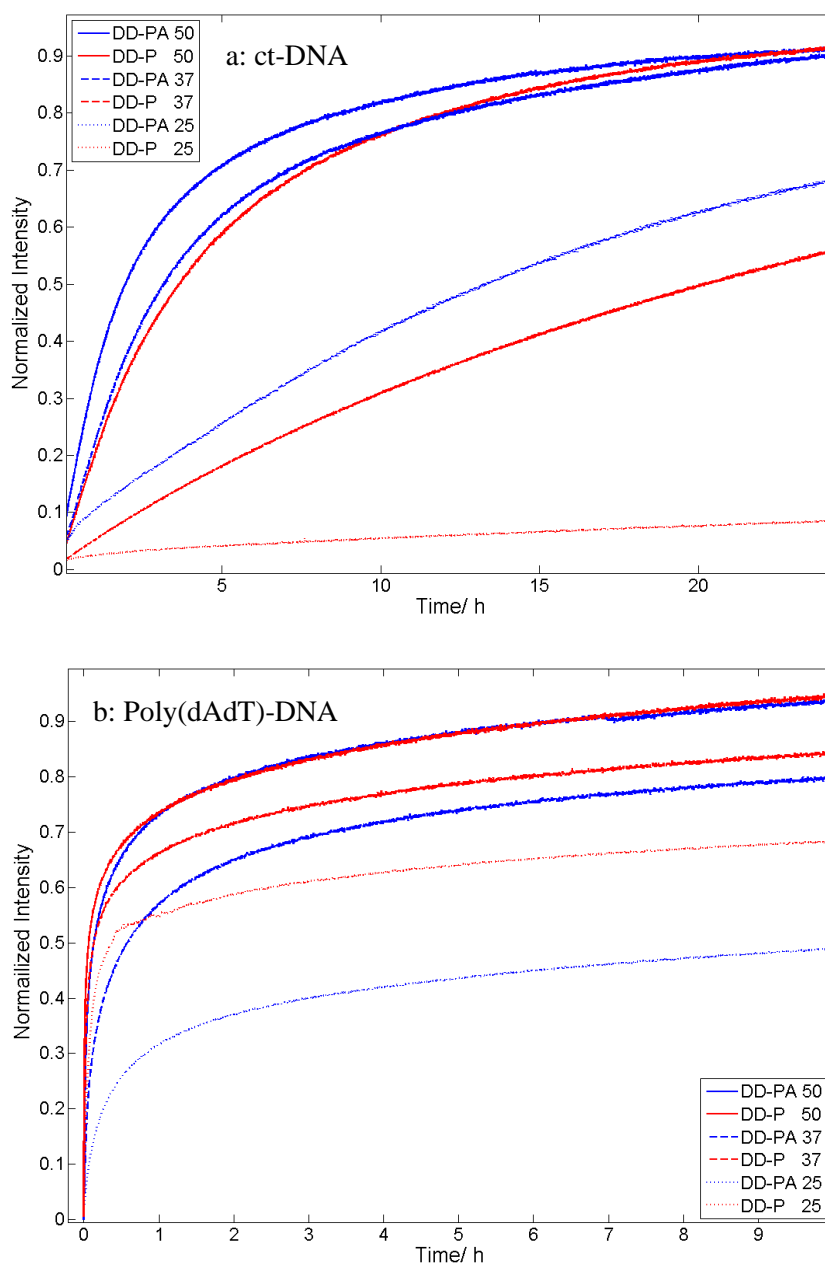


Fig 4.7 the kinetics measurements with ct-DNA and poly (dAdT)<sub>2</sub> DNA of  $\Delta,\Delta$ -P and  $\Delta,\Delta$ -PA in 50, 37 and 25 °C. a: the kinetics of  $\Delta,\Delta$ -PA and  $\Delta,\Delta$ -P measurements with ct-DNA; b: the kinetics of  $\Delta,\Delta$ -PA and  $\Delta,\Delta$ -P measurements with poly (dAdT)<sub>2</sub>-DNA

#### 4.10 Dissociation Kinetics

SDS sequestered dissociation was measured followed by the kinetics measurement. P and PA dissociation from ct-DNA and poly (dAdT)<sub>2</sub> DNA were measured in different temperature (Data are presented in Appendix). Fig 4.8 shows the time-based fluorescence dissociation measurements.

a: ct-DNA 50 °C

b: ct-DNA 37 °C

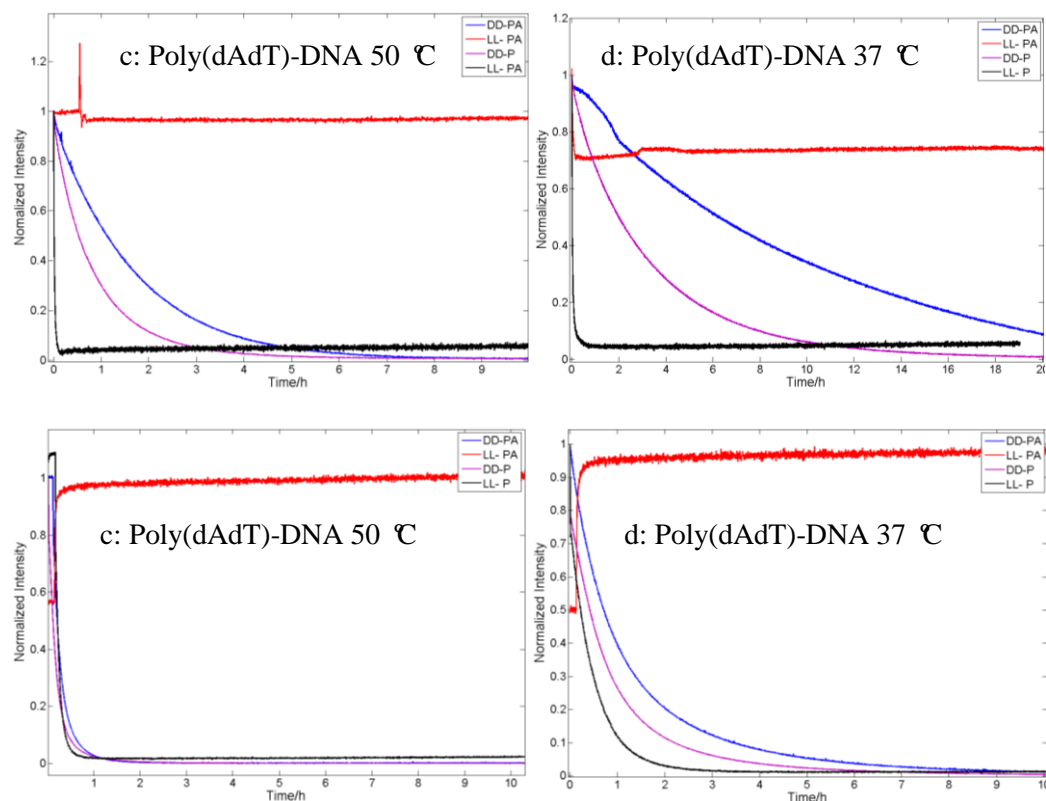


Fig 4.8 the dissociation measurements of different complexes in different temperatures with ct-DNA and poly (dAdT)<sub>2</sub> DNA

From the plot,  $\Delta, \Delta$ -P release so fast that it is difficult to compare with others. As the associations,  $\Delta, \Delta$ -PA is meaningless to analysis.  $\Delta, \Delta$ -PA is slower release compared with  $\Delta, \Delta$ -P from ct-DNA for both 50 and 37 °C. However,  $\Delta, \Delta$ -PA is the same dissociation rate with  $\Delta, \Delta$ -P at 50 °C from poly (dAdT)<sub>2</sub> DNA, and  $\Delta, \Delta$ -PA is a little bit slower release rate than  $\Delta, \Delta$ -P from poly (dAdT)<sub>2</sub> DNA at 37 °C.

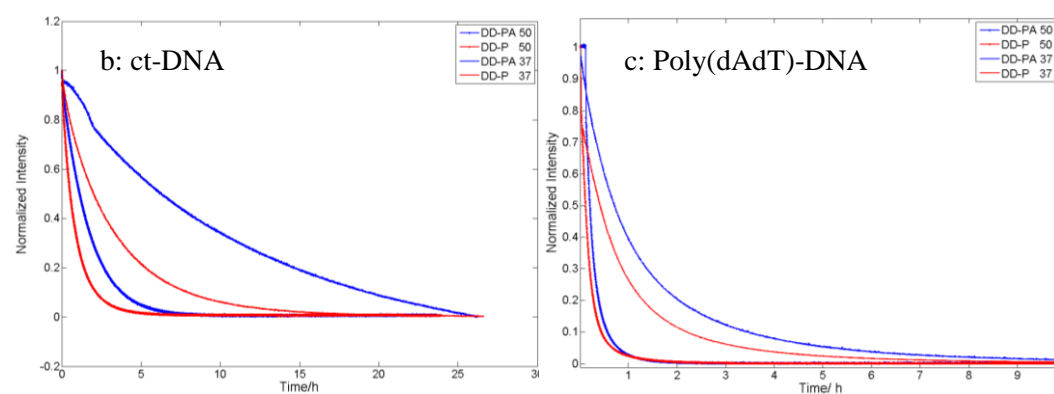


Fig 4.9 the dissociation comparison between  $\Delta, \Delta$ -P and  $\Delta, \Delta$ -PA at 37 and 50 C from ct-DNA and poly (dAdT)<sub>2</sub> DNA

Temperature is more important for dissociation from ct-DNA than that from poly (dAdT)<sub>2</sub> DNA. See Fig 4.9, the release rate of PA is significantly more affected by temperature from ct-DNA. The distinguishing can be apparently observed from the Fig 4.9 a. The same results were appeared for the poly (dAdT)<sub>2</sub> DNA, much more impacts by temperature variation with the rate of release for  $\Delta,\Delta$ -PA. For  $\Delta,\Delta$ -PA, here is a lower energy barrier of association kinetics and higher energy barrier of dissociation kinetics compared with  $\Delta,\Delta$ -P.



## 5. Conclusion

The purpose of this thesis is to investigate the binding mode and kinetic selectivity of PA, which is the elongating bridge length of binuclear complex, the enantiomer of P as the reference to compare the results.

### 5.1 Binding Mode

Through different physical techniques such as Absorption Linear Dichroism and Circular Dichroism, the bonding modes are quite different for two enantiomers of PA.

- Threading intercalation seems to be the binding mode of  $\Delta,\Delta$ -PA. The binding bridge is oriented roughly perpendicular to the helix axis, which is in agreement with the observation of the earlier interactions of the  $\Delta,\Delta$ - and  $\Lambda,\Lambda$ -P.
- No observable evidence proved that threading intercalation is the binding mode of  $\Lambda,\Lambda$ -PA with DNA.

### 5.2 Kinetics

Time-based fluorescence measurement was used to investigate the binding process:

- $\Delta,\Delta$ -PA bound to ct-DNA helix, and a faster threading intercalation is shown than  $\Lambda,\Lambda$ -P. But a slower unthreading process of  $\Delta,\Delta$ -PA is observed than  $\Lambda,\Lambda$ -P from ct-DNA. Temperature has a larger impact on  $\Delta,\Delta$ -PA than  $\Lambda,\Lambda$ -P.
- Compared with P, PA is less AT-sequence selective but still PA has a stronger affinity for poly(dAdT)<sub>2</sub> DNA than ct-DNA. The binding rate of  $\Delta,\Delta$ -PA is similar in high temperature (50 °C) with  $\Lambda,\Lambda$ -P. For unthreading process, a similar release rate between P and PA in high temperature, but with the temperature decrease, the release rate of  $\Delta,\Delta$ -PA gets slower than  $\Lambda,\Lambda$ -P.

Considering the faster threading process than unthreading process compared with  $\Lambda,\Lambda$ -P,  $\Delta,\Delta$ -PA is a stronger intercalator.



## 6. Acknowledgement

Now, I would express my sincere gratitude to everyone who helped me and supported me during this thesis. First, I am really grateful to my supervisor Johanna Andersson and examiner Per Lincoln.

Per, thanks for allowing me to join in your research group to finish my diploma work. In truth, I learned so much and experienced a wonderful time with a lot of happiness. Thanks for your patient guidance, expert advice and inspiration encouragement, always.

Johanna, you are really a nice supervisor and mentor. I must thank for your comprehensive explanation and careful correction of my report. Thank you for giving me a lot of suggestions of my experiment process and teaching me many useful experimental skills.

Here, I must delivery my gratitude to Pär Nordell. Though we even do not have a face to face talking, I acquired huge of information and assistance from your report.

Special thanks for Calin and Yang Chi, my good opponents read my report and help me to correct minor mistakes and improve my poor written English. Bobo, thanks for your scientific suggestions, valuable recommendations and patient help in this half a year. Thank you all other diploma workers for being a nice roommate to share this short time.

I have to thank you all who work in 5<sup>th</sup> floor, thank you of your help and uncomplaining support of my work. Also, thank you, all my friends who support me and courage me when I stay in abroad for my master program.

Finally, I dedicate all my gratitude to my parents. Thank you for your unshakable faith in me.

Yubo Wang

in Göteborg, Sweden, 2010



## 7. References

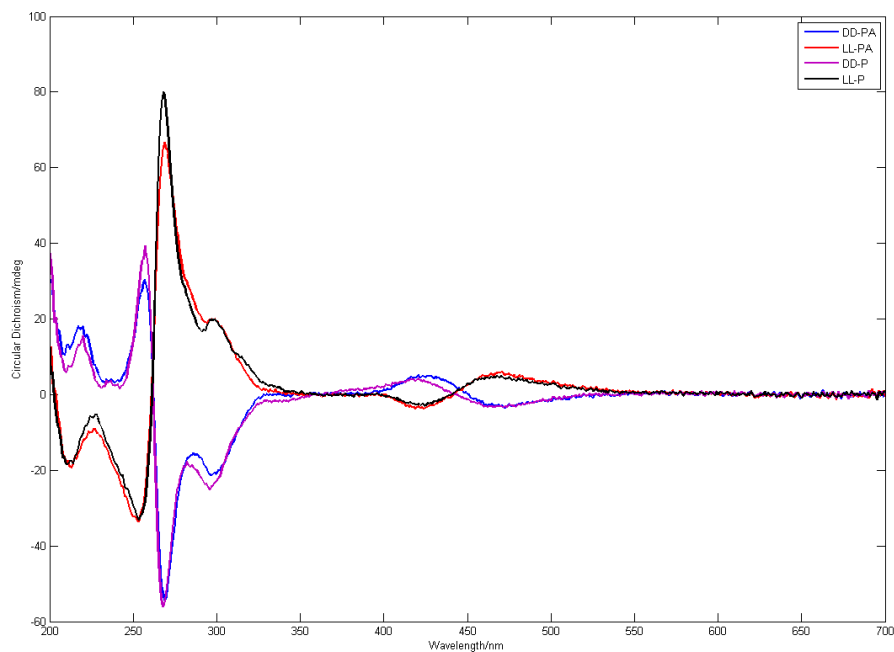
1. Hershey, A.D. and M. Chase, *Independent functions of viral protein and nucleic acid in growth of bacteriophage*. J Gen Physiol, 1952. **36**(1): p. 39-56.
2. Watson, J.D. and F.H. Crick, *The structure of DNA*. Cold Spring Harb Symp Quant Biol, 1953. **18**: p. 123-31.
3. Meselson, M. and F.W. Stahl, *The Replication of DNA in Escherichia Coli*. Proc Natl Acad Sci U S A, 1958. **44**(7): p. 671-82.
4. Lagerkvist, U., [*The 1968 Nobel prize in physiology or medicine. The genetic code and its translation*]. Lakartidningen, 1968. **65**(44): p. 4373-81.
5. Lander, E.S. and etc., *Initial sequencing and analysis of the human genome*. Nature, 2001. **409**(6822): p. 860-921.
6. Venter, J.C. and etc., *The sequence of the human genome*. Science, 2001. **291**(5507): p. 1304-51.
7. Gibson, D., *Drug-DNA interactions and novel drug design*. Pharmacogenomics J, 2002. **2**(5): p. 275-6.
8. Cho-Chung, Y.S., *DNA drug design for cancer therapy*. Curr Pharm Des, 2005. **11**(22): p. 2811-23.
9. Fernandez, A. and S. Sessel, *Selective antagonism of anticancer drugs for side-effect removal*. Trends Pharmacol Sci, 2009. **30**(8): p. 403-10.
10. Ahmad, S., *Platinum-DNA Interactions and Subsequent Cellular Processes Controlling Sensitivity to Anticancer Platinum Complexes*. Chem Biodivers. **7**(3): p. 543-566.
11. Brown, S.D., et al., *Gold Nanoparticles for the Improved Anticancer Drug Delivery of the Active Component of Oxaliplatin*. J Am Chem Soc.
12. Christopher K. Mathews, K.E.V.H., Kevin G. Ahern, ed. *Biochemistry*. 2000.
13. Moreau, J., L. Matyash-Smirniaguina, and K. Scherrer, *Systematic punctuation of eukaryotic DNA by A+T-rich sequences*. Proc Natl Acad Sci U S A, 1981. **78**(3): p. 1341-5.
14. Moreau, J., et al., *A + T-rich linkers define functional domains in eukaryotic DNA*. Nature, 1982. **295**(5846): p. 260-2.
15. Moreau, J., et al., *AT-rich linkers in long range organisation of Drosophila DNA*. Mol Gen Genet, 1985. **199**(3): p. 357-64.
16. Israelewski, N., *Structure and function of an AT-rich, interspersed repetitive sequence from Chironomus thummi: solenoidal DNA, 142 bp palindrome-frame and homologies with the sequence for site-specific recombination of bacterial transposons*. Nucleic Acids Res, 1983. **11**(20): p. 6985-96.
17. Woynarowski, J.M., M. Krugliak, and H. Ginsburg, *Pharmacogenomic analyses of targeting the AT-rich malaria parasite genome with AT-specific alkylating drugs*. Mol Biochem Parasitol, 2007. **154**(1): p. 70-81.
18. Anthony, D.A. and C.J. Twelves, *DNA: still a target worth aiming at? A review of new DNA-interactive agents*. Am J Pharmacogenomics, 2001. **1**(1): p. 67-81.

19. Schmidt, C.E., et al., [*University clinics in the competitive hospital market*]. *Anaesthesist*, 2005. **54**(7): p. 694-702.
20. Lerman, L.S., *Structural considerations in the interaction of DNA and acridines*. *J Mol Biol*, 1961. **3**: p. 18-30.
21. Chaires, J.B., *Energetics of drug-DNA interactions*. *Biopolymers*, 1997. **44**(3): p. 201-15.
22. Bischoff, G. and S. Hoffmann, *DNA-binding of drugs used in medicinal therapies*. *Curr Med Chem*, 2002. **9**(3): p. 312-48.
23. Palchaudhuri R, H.P., *DNA as a target for anticancer compounds: methods to determine the mode of binding and the mechanism of action*. *Curr Opin Biotechnol.*, 2007. **18**(6): p. 497-503.
24. Patel, M.N., P.A. Parmar, and D.S. Gandhi, *Square pyramidal copper(II) complexes with forth generation fluoroquinolone and neutral bidentate ligand: structure, antibacterial, SOD mimic and DNA-interaction studies*. *Bioorg Med Chem*, 2010. **18**(3): p. 1227-35.
25. Tarushi, A., et al., *Zinc(II) complexes of the second-generation quinolone antibacterial drug enrofloxacin: Structure and DNA or albumin interaction*. *Bioorg Med Chem*, 2010. **18**(7): p. 2678-85.
26. Vandiver, M.S., et al., *Effect of ancillary ligands on the DNA interaction of [Cr(diimine)<sub>3</sub>]<sup>3+</sup> complexes containing the intercalating dipyridophenazine ligand*. *Inorg Chem*, 2010. **49**(3): p. 839-48.
27. Jacqueline K. Barton, A.T.D., and Jonathan M. Goldberg, *Tris(phenanthroline)ruthenium(II): Stereoselectivity in Binding to DNA*. *J. Am. Chem. SO*, 1984. **106**(7): p. 2172-2176.
28. Challa V. Kumar, J.K.B., and Nicholas J. Turro, *Photophysics of Ruthenium Complexes Bound to Double Helical DNA*. *J. Am. Chem. Soc.*, 1985. **107**(19): p. 5518-5523.
29. Jacqueline K. Barton, J.M.G., Challa V. Kumar, and Nicholas J. Turro, *Binding Modes and Base Specificity of Tris(phenanthroline)ruthenium(II) Enantiomers with Nucleic Acids: Tuning the Stereoselectivity*. *J. Am. Chem. Soc.*, 1986. **108**(8): p. 2081-2088.
30. Jacqueline K. Barton, A.T.D., and Jonathan M. Goldberg,, *Tris(phenanthroline)ruthenium(II): Stereoselectivity in Binding to DNA*. *J. Am. Chem. SO*, 1984. **106**(7): p. 2172-2176.
31. Catarina Hiort, B.N.a.A.R., *Enantiopreferential DNA Binding of [Ru<sup>II</sup>(1,10-phenanthroline)<sub>3</sub>]<sup>2+</sup> Studied with Linear and Circular Dichroism*. *J. Am. Chem. SO*, 1990. **112**(5): p. 1971-1982.
32. Satyanarayana, S., J.C. Dabrowiak, and J.B. Chaires, *Tris(phenanthroline)ruthenium(II) enantiomer interactions with DNA: mode and specificity of binding*. *Biochemistry*, 1993. **32**(10): p. 2573-84.
33. Jenkins, Y., et al., *Characterization of dipyridophenazine complexes of ruthenium(II): the light switch effect as a function of nucleic acid sequence and conformation*. *Biochemistry*, 1992. **31**(44): p. 10809-16.

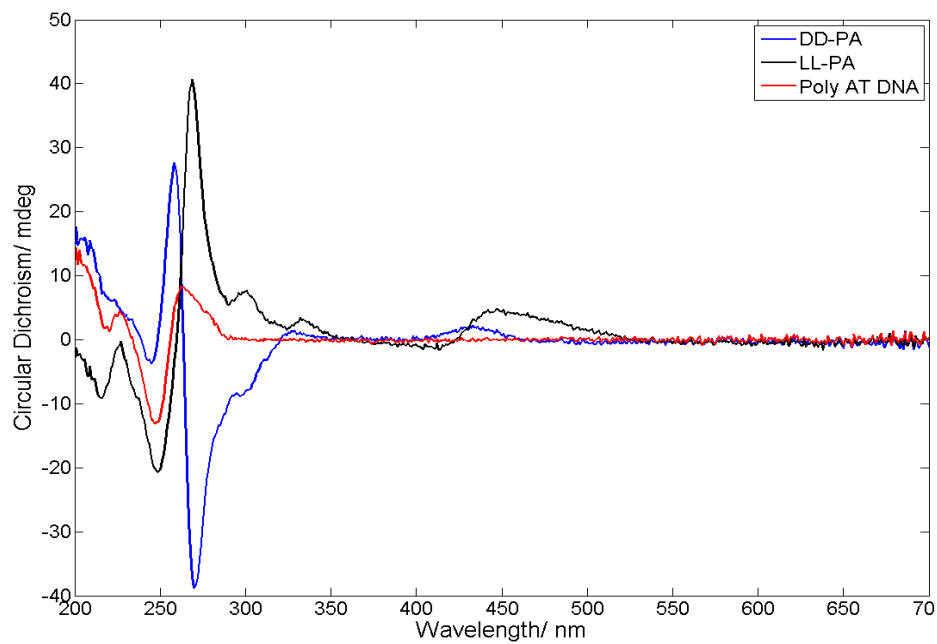
34. Catarina Hiort, P.L.a.B.N., *DNA Binding of  $\Delta$ - and  $\Lambda$ -[Ru(phen)<sub>2</sub>DPPZ]<sup>2+</sup>*. J. Am. Chem. SO, 1993. **115**(9): p. 3448-3454.
35. Haq I, L.P., Suh DC, Norden B, Chowdhry BZ, Chaires JB, *Interaction of Delta-(Ru(Phen)(2)Dppz)(2+) and Lambda-(Ru(Phen)(2)Dppz)(2+) with DNA - A Calorimetric and Equilibrium Binding Study*. J. Am. Chem. SO, 1995. **117**(17): p. 4788-4796.
36. Alan E. Friedman, J.-C.C., Jean-Pierre Sauvage, Nicholas J. Turro and Jacqueline K. Barton, *Molecular "Light Switch" for DNA Ru(bpy)<sub>2</sub>(dppz)<sup>2+</sup>*. J. Am. Chem. SO, 1990. **112**: p. 4960-4962.
37. Wilhelmsson, L.M., et al., *DNA-binding of semirigid binuclear ruthenium complex delta,delta-[mu-(11,11'-bidppz)(phen)(4)ru(2)](4+): extremely slow intercalation kinetics*. J Am Chem Soc, 2002. **124**(41): p. 12092-3.
38. Westerlund, F., et al., *Binding geometry and photophysical properties of DNA-threading binuclear ruthenium complexes*. J Phys Chem B, 2007. **111**(1): p. 310-7.
39. Westerlund, F., et al., *Complex DNA binding kinetics resolved by combined circular dichroism and luminescence analysis*. J Phys Chem B, 2008. **112**(21): p. 6688-94.
40. Wilhelmsson, L.M., E. K. Esbjörner, F. Westerlund, B. Nordén and P. Lincoln, *meso stereoisomer as a probe of enantioselective threading intercalation of aemirigid ruthenium complex [μ-(11,11'-bidppz)(phen)<sub>4</sub> Ru<sub>2</sub>]<sup>4+</sup>*. J.Physical Chemistry B, 2003. **107**(42): p. 11784-11793.
41. Nordell, P. and P. Lincoln, *Mechanism of DNA threading intercalation of binuclear Ru complexes: uni- or bimolecular pathways depending on ligand structure and binding density*. J Am Chem Soc, 2005. **127**(27): p. 9670-1.
42. Rodger, A. and B. Nordén, *Circular Dichroism and Linear Dichroism*. 1997.
43. Carlos.RC. Available from:  
[http://upload.wikimedia.org/wikipedia/commons/0/04/Beer\\_lambert.png](http://upload.wikimedia.org/wikipedia/commons/0/04/Beer_lambert.png).
44. Forster, L.S., *Fluorescence lifetimes of biomolecules*. Photochem Photobiol, 1976. **23**(6): p. 445-8.
45. Lakowicz, J.R., ed. *Principles of fluorescence spectroscopy*. ed. r. edition. September 15, 2006.
46. Takahashi, M., M. Kubista, and B. Norden, *Binding of recA protein to Z-form DNA studied with circular and linear dichroism spectroscopy*. J Biol Chem, 1989. **264**(15): p. 8568-74.
47. Arnott, S. and D.W. Hukins, *Conservation of conformation in mono and polynucleotides*. Nature, 1969. **224**(5222): p. 886-8.
48. Arrhenius, S.A., *Über den Reaktionsgeschwindigkeit bei der Inversion von Rohrzucker durch Säuren*. Z.phys.Chem, 1889. **4**: p. 226-248.
49. Per Lincoln, B.N., *Binuclear ruthenium(II) phenanthroline compounds with extreme binding affinity for DNA*. Chem. Commun., 1996: p. 2145-2146.
50. Joseph B. Lambert, H.F.S., David A. Lightner, R. Graham Cooks, ed. *Organic Structural Spectroscopy*. 2001.
51. Per Lincoln, A.B., and Bengt Nordén, *Diastereomeric DNA-binding geometries of intercalated ruthenium(II) trischelates probed by linear dichroism:*

*[Ru(phen)<sub>2</sub>DPPZ]<sup>2+</sup> and [Ru(phen)<sub>2</sub>BDPPZ]<sup>2+</sup>*. J. Am. Chem. SO, 1996. **118**: p. 2644-2653.

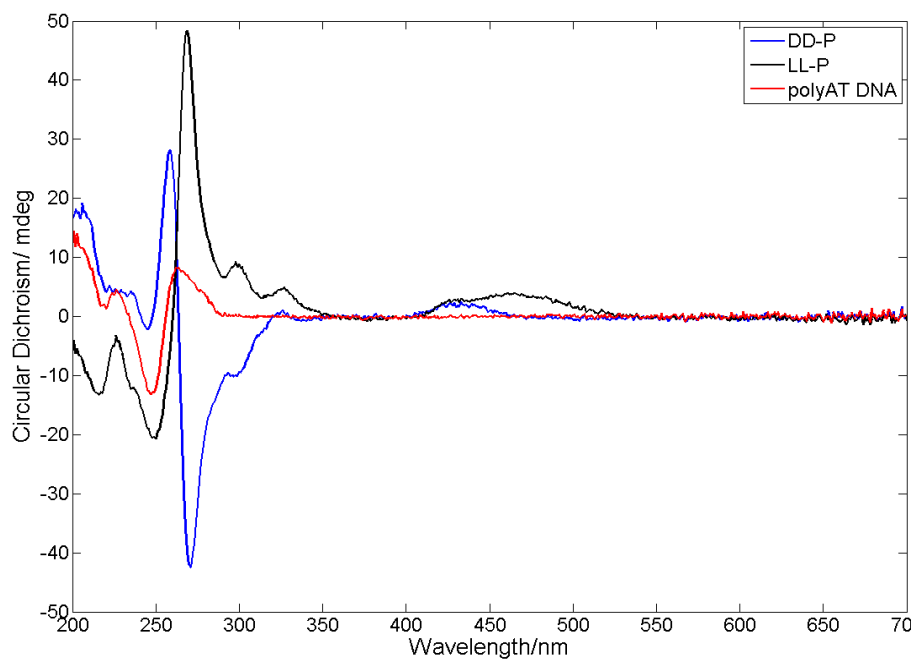
## Appendix I



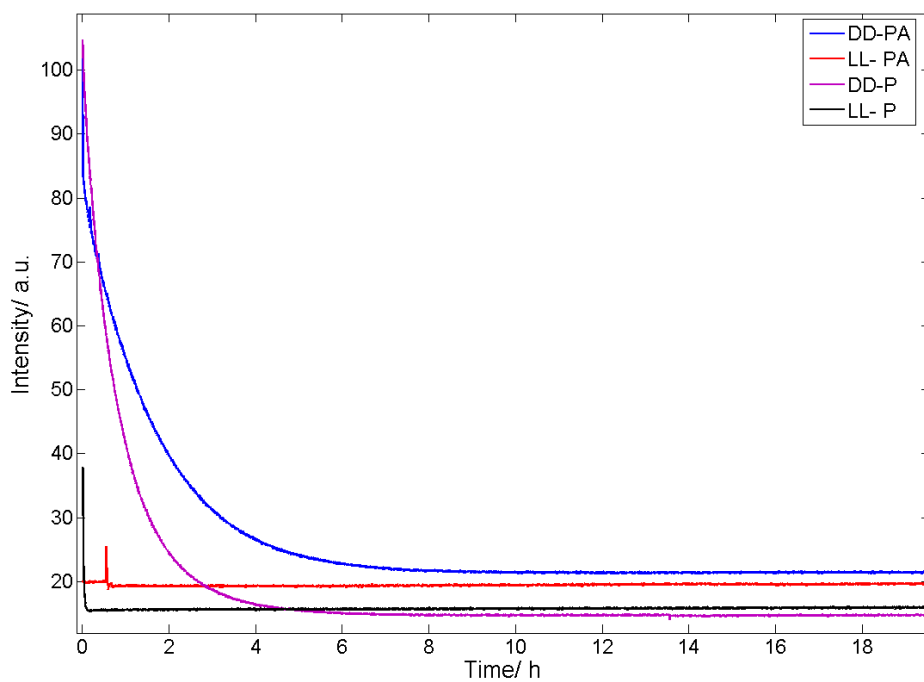
CD spectrum of pure complexes P and PA



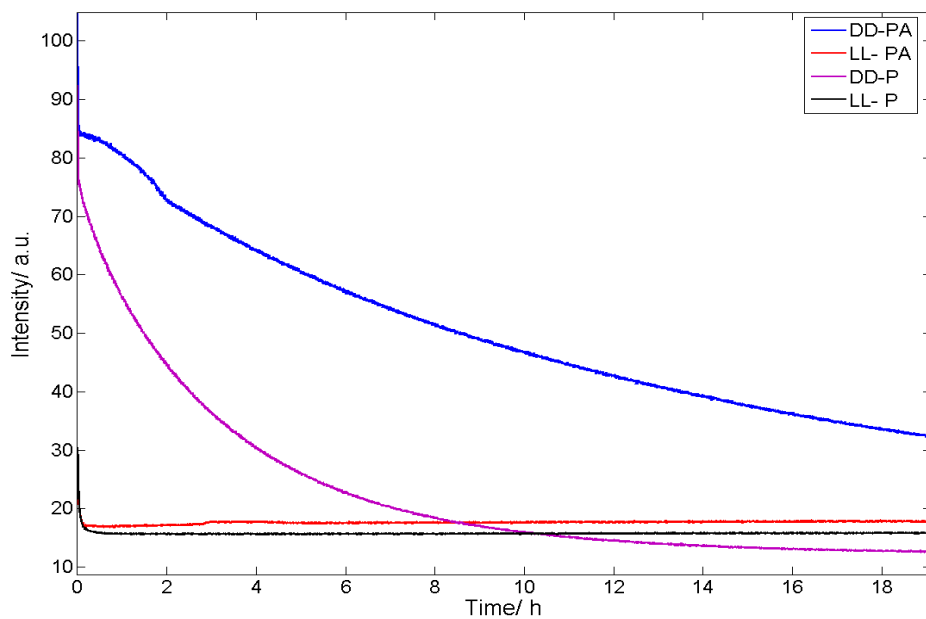
CD spectrum of complexes PA interact with poly(dAdT)<sub>2</sub> DNA after heated at 50 °C



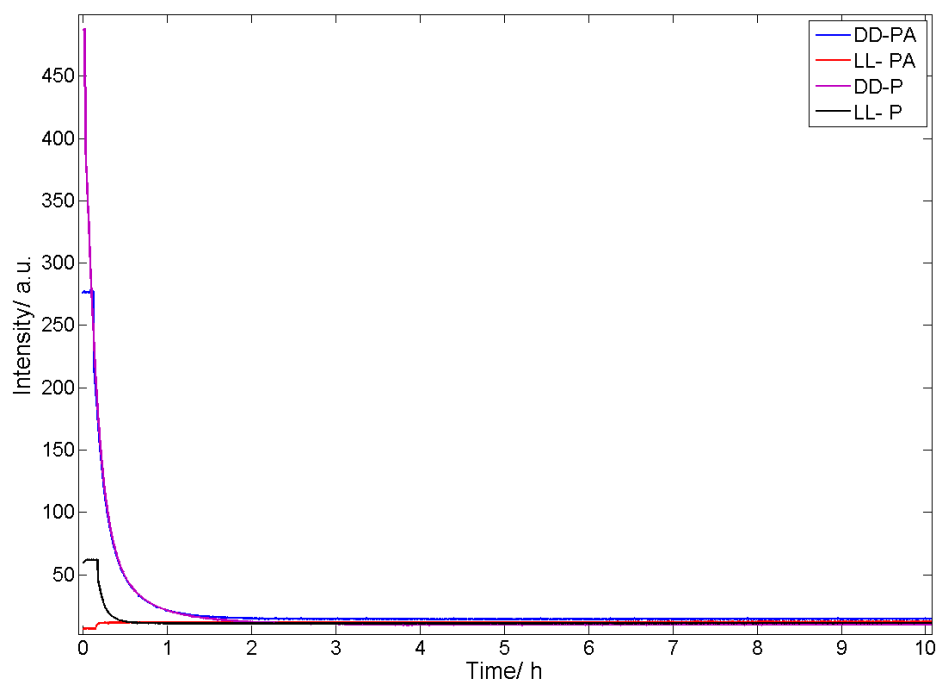
CD spectrum of complexes P interact with poly(dAdT)<sub>2</sub> DNA after heated at 50 °C



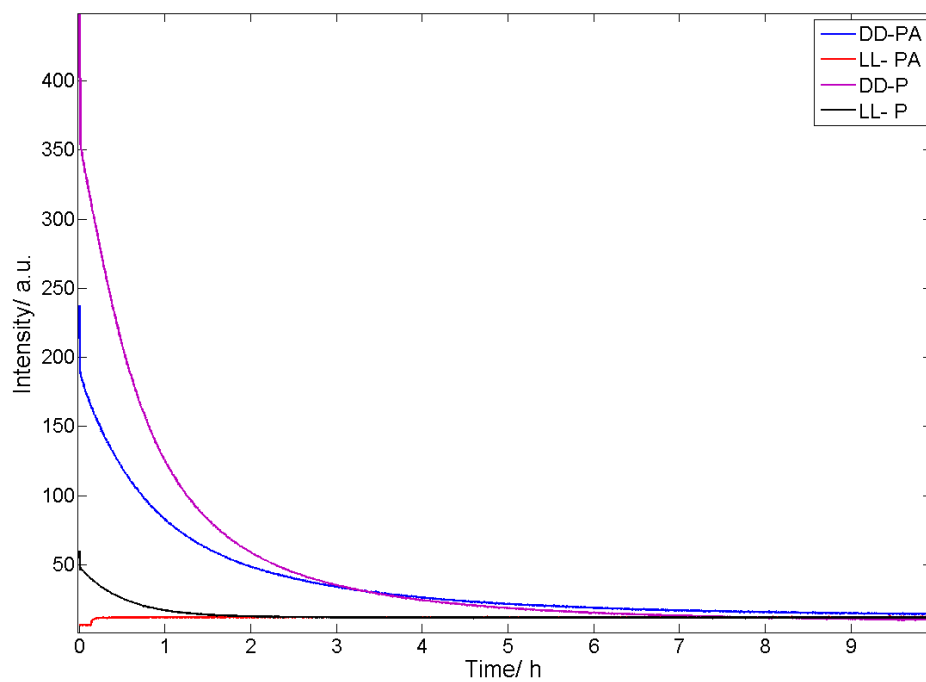
The raw dissociation kinetics data for ct-DNA at 50 °C



The raw dissociation kinetics data for ct-DNA at 37 °C



The raw dissociation kinetics data for poly(dAdT)<sub>2</sub> DNA at 50 °C



The raw dissociation kinetics data for poly(dAdT)<sub>2</sub> DNA at 37 °C

## Appendix II

DNA	T( °C)	model	(min)	$\Delta,\Delta$ -PA	$\Delta,\Delta$ -P	$\Lambda,\Lambda$ -PA	$\Lambda,\Lambda$ -P
ct-DNA	37	1-exponential	$\tau$	419.4	1579.8	907.8	380.4
		2-exponential	$\tau_1(\alpha_1)$	160.2(0.62)	274.3(0.05)	546.67(0.39)	98.9(0.3)
			$\tau_2(\alpha_2)$	1137.5(0.38)	1792.2(0.95)	5333.3(0.61)	616.2(0.7)
			Ave $\tau$	531.57	1716.3	3466.5	461.01
	45	1-exponential	$\tau$	185.3	442.1	292.5	241.88
		2-exponential	$\tau_1(\alpha_1)$	99.1(0.67)	212.3(0.33)	6.6(0.03)	64.7(0.44)
			$\tau_2(\alpha_2)$	517.8(0.33)	680.4(0.67)	291.3(0.97)	415(0.56)
			Ave $\tau$	237.27	525.93	282.76	338.83
	50	1-exponential	$\tau$	218.85	331.38	259.9	58.58
		2-exponential	$\tau_1(\alpha_1)$	95.7(0.42)	145.6(0.63)	121.77(0.6)	18.55(0.83)
			$\tau_2(\alpha_2)$	580.5(0.58)	532.2(0.37)	641.57(0.4)	222.17(0.17)
			Ave $\tau$	376.9	288.6	329.7	53.17

Table the association data of complexes bound to ct-DNA

Poly (dAdT) <sub>2</sub> DNA	25	1-exponential	$\tau$	342.40	249.40	182.17	182.17
		2-exponential	$\tau_1(\alpha_1)$	32.00(0.55)	7.30(0.90)	45.20(0.66)	19.80(0.73)
			$\tau_2(\alpha_2)$	645.62(0.45)	374.65(0.10)	360.80(0.34)	365.22(0.27)
			Ave $\tau$	308.13	44.04	152.50	130.41
	37	1-exponential	$\tau$	78.68	98.00	14.52	114.80
		2-exponential	$\tau_1(\alpha_1)$	13.90(0.63)	5.30(0.72)	8.00(0.85)	17.97(0.72)
			$\tau_2(\alpha_2)$	190.47(0.37)	199.50(0.28)	139.36(0.15)	232.15(0.28)
			Ave $\tau$	79.23	59.68	27.70	77.94
	50	1-exponential	$\tau$	45.25	101.30	19.40	50.00
		2-exponential	$\tau_1(\alpha_1)$	10.50(0.73)	4.50(0.71)	-	12.60(0.85)
			$\tau_2(\alpha_2)$	183.70(0.27)	191.40(0.29)	-	241.80(0.15)
			Ave $\tau$	57.26	58.70	-	46.98

Table the association data of complexes bound to poly (dAdT)<sub>2</sub> DNA

DNA	Temperature	model	(Min)	$\Delta,\Delta$ -PA	$\Delta,\Delta$ -P	$\Lambda,\Lambda$ -PA	$\Lambda,\Lambda$ -P
ct-DNA	37	1-exponential	$\tau$	630	198.1	11.1	2.73
		2-exponential	$\tau_1(\alpha_1)$	25(0.30)	29.9(0.14)	-	-
			$\tau_2(\alpha_2)$	737.55(0.70)	241(0.86)	-	-
			Ave $\tau$	523.8	211.4	-	-
	50	1-exponential	$\tau$	98.5	51.3	21.88	1.0
		2-exponential	$\tau_1(\alpha_1)$	-	-	-	-
			$\tau_2(\alpha_2)$	-	-	-	-
		Ave $\tau$	-	-	-	-	

Table the dissociation data of complexes release from ct-DNA

Poly (dAdT) <sub>2</sub> DNA	25	1-exponential	$\tau$	366.8	214.3	-	82.1
		2-exponential	$\tau_1(\alpha_1)$	163.0(0.46)	105.9(0.60)	-	60.4(0.75)
			$\tau_2(\alpha_2)$	874.0(0.54)	463.6(0.40)	-	154.0(0.25)
			Ave $\tau$	475.8	249.0		83.8
	37	1-exponential	$\tau$	58.7	51.3	8.5	30.7
		2-exponential	$\tau_1(\alpha_1)$	13.3(0.38)	3.4(0.25)	-	-
			$\tau_2(\alpha_2)$	82.72(0.62)	56.3(0.75)	-	-
			Ave $\tau$	56.34	43.1	-	-
	50	1-exp	$\tau$	14.0	10.5	9.2	11.6
		2-exp	$\tau_1(\alpha_1)$	-	-	-	-
			$\tau_2(\alpha_2)$	-	-	-	-
			Ave $\tau$		-	-	-

Table the dissociation data of complexes release from poly (dAdT)<sub>2</sub> DNA